THE JOURNAL OF PHYSICAL CHEMISTRY A
A JOURNAL OF THE AMERICAN CHEMICAL SOCIETY

pubs.acs.org/JPCA Article

Reference Energies for Cyclobutadiene: Automerization and Excited States

Enzo Monino,* Martial Boggio-Pasqua, Anthony Scemama, Denis Jacquemin, and Pierre-François Loos*

Cite This: *J. Phys. Chem. A* 2022, 126, 4664−4679 Read Online

ACCESS | Metrics & More | Article Recommendations | Supporting Information

ABSTRACT: Cyclobutadiene is a well-known playground for theoretical chemists and is particularly suitable to test ground- and excited-state methods. Indeed, due to its high spatial symmetry, especially at the D_{4h} square geometry but also in the D_{2h} rectangular arrangement, the ground and excited states of cyclobutadiene exhibit multiconfigurational characters and single-reference methods, such as standard adiabatic time-dependent density-functional theory (TD-DFT) or standard equation-of-motion coupled cluster (EOM-CC), are notoriously known to struggle in such situations. In this work, using a large panel of methods and basis sets, we provide an extensive computational study of the automerization barrier (defined as the difference between the square and rectangular ground-state energies) and the vertical excitation energies at D_{2h} and D_{4h} equilibrium structures. In particular, selected configuration interaction (SCI), multireference perturbation theory (CASSCF, CASPT2, and NEVPT2), and coupled-cluster (CCSD, CC3, CCSDT, CC4, and CCSDTQ) calculations are performed. The spin-flip formalism, which is known to provide a qualitatively correct description of these diradical states, is also tested within TD-DFT (combined with numerous exchange-correlation functionals) and the algebraic diagrammatic construction [ADC(2)-s, ADC(2)-x, and ADC(3)]. A theoretical best estimate is defined for the automerization barrier and for each vertical transition energy.

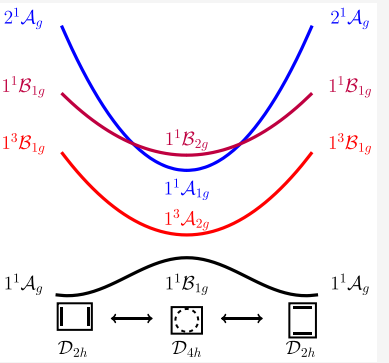

1. INTRODUCTION

Despite the fact that excited states are involved in ubiquitous processes such as photochemistry,[1−7] catalysis,[8] and solar cells,[9] none of the currently existing methods have shown to provide accurate excitation energies in all scenarios due to the complexity of the process, the size of the systems, the impact of the environment, and many other factors. Indeed, each computational model has its own theoretical and/or technical limitations, and the number of possible chemical scenarios is so vast that the design of new excited-state methodologies remains a very active field of theoretical quantum chemistry.[10−23]

Speaking of difficult tasks, the cyclobutadiene (CBD) molecule has been a real challenge for both experimental chemistry and theoretical chemistry for many decades.[24] Due to its antiaromaticity[25] and large angular strain,[26] CBD presents a high reactivity making its synthesis a particularly difficult exercise. In the D_{4h} symmetry, the simple Hückel molecular orbital theory wrongly predicts a triplet ground state (Hund's rule) with two singly occupied frontier orbitals that are degenerate by symmetry, while state-of-the-art *ab initio* methods correctly predict an open-shell singlet ground state. This degeneracy is lifted by the so-called pseudo-Jahn−Teller effect, i.e., by a descent in symmetry (from D_{4h} to D_{2h} point group) via a geometrical distortion of the molecule, leading to a closed-shell singlet ground state in the rectangular geometry (see below). This was confirmed by several experimental studies by Pettis and co-workers[27] and others.[28−30]

In the D_{2h} symmetry, the 1^1A_g ground state has a weak multiconfigurational character with well-separated frontier orbitals that can be described by single-reference methods. However, in the D_{4h} symmetry, the 1^1B_{1g} ground state is a diradical that has two degenerate singly occupied frontier orbitals. Therefore, one must take into account, at least, two electronic configurations to properly model this multiconfigurational scenario. Of course, standard single-reference methods are naturally unable to describe such situations. Interestingly, the 1^1B_{1g} ground state of the square arrangement is a transition state in the automerization reaction between the two rectangular structures (see Figure 1), while the lowest triplet state, 1^3A_{2g}, is a minimum on the triplet potential energy surface in the D_{4h} arrangement. The automerization barrier (AB) is thus defined as the difference between the square and rectangular ground-state energies. The energy of this barrier is estimated, experimentally, in the range of 1.6−10 kcal mol^{-1},[31] while previous state-of-the-art *ab initio* calculations yield values in the 7−9 kcal mol^{-1} range.[32−35]

Received: April 11, 2022
Revised: June 30, 2022
Published: July 12, 2022

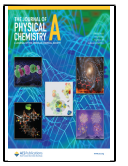

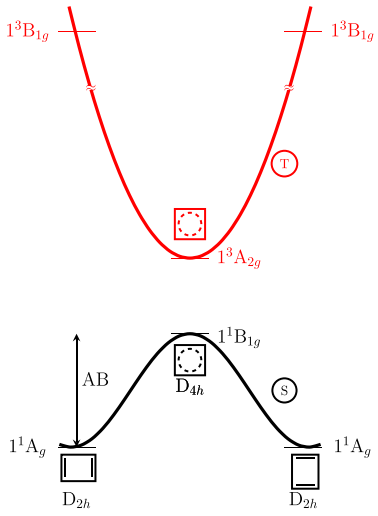

Figure 1. Pictorial representation of the ground and lowest excited states of CBD and the properties under investigation. The singlet (S) and triplet (T) ground-state properties are colored in black and red, respectively. The automerization barrier (AB) is also represented.

The lowest-energy excited states of CBD in both symmetries are represented in Figure 1, where we have reported the 1^1A_g and 1^3B_{1g} states for the rectangular geometry and the 1^1B_{1g} and 1^3A_{2g} states for the square one. Due to the energy scale, the higher-energy states (1^1B_{1g} and 2^1A_g for D_{2h} and 1^1A_{1g} and 1^1B_{2g} for D_{4h}) are not shown. Interestingly, the 2^1A_g and 1^1A_{1g} states have a strong contribution from doubly excited configurations, and these so-called double excitations[36] are known to be inaccessible with standard adiabatic time-dependent density-functional theory (TD-DFT)[37−45] and remain challenging for the standard hierarchy of equation-of-motion coupled cluster (EOM-CC) methods that are using ground-state Hartree−Fock reference.[46−49]

In order to tackle the problem of multiconfigurational character and double excitations, we have explored several approaches. The most evident way is to rely on multireference methods, which are naturally designed to address such scenarios. Among these methods, one can mention the complete-active-space self-consistent field (CASSCF) method,[10] its second-order perturbatively corrected variant (CASPT2),[50−52] and the second-order *n*-electron valence state perturbation theory (NEVPT2) formalism.[53−55]

Another way to deal with double excitations and multireference situations is to use high level truncation of the EOM formalism[56,57] of CC theory.[46−49,58] However, to provide a correct description of these situations, one has to take into account, at the very least, contributions from the triple excitations in the CC expansion.[36,59−61] Although multireference CC methods have been designed,[62−66] they are computationally demanding and remain far from being black box.

In this context, an interesting alternative to multireference and CC methods is provided by selected configuration interaction (SCI) methods,[67−80] which are able to provide near full CI (FCI) ground- and excited-state energies of small molecules.[36,60,61,81−98] For example, the *Configuration Interaction using a Perturbative Selection made Iteratively* (CIPSI) method limits the exponential increase of the size of the CI expansion by retaining the most energetically relevant determinants only, using a second-order energetic criterion to select perturbatively determinants in the FCI space.[69,70,72,80,92,99] Nonetheless, SCI methods remain very expensive and can be applied to a limited number of situations.

Finally, another option to deal with these chemical scenarios is to rely on the spin-flip formalism, established by Krylov in 2001,[100−103] where one accesses the ground and doubly excited states via a single (spin-flip) de-excitation and excitation from the lowest triplet state, respectively. One drawback of spin-flip methods is spin contamination (i.e., the artificial mixing of electronic states with different spin multiplicities) due not only to the spin incompleteness in the spin-flip expansion but also to the potential spin contamination of the reference configuration.[103] One can address part of this issue by increasing the excitation order or by complementing the spin-incomplete configuration set with the missing configurations.[104−111] Note that one can quantify the polyradical character associated with a given electronic state using Head-Gordon's index[112] that provides a measure of the number of unpaired electrons.[113]

In the present work, we define highly accurate reference values and investigate the accuracy of each family of computational methods mentioned above on the automerization barrier and the low-lying excited states of CBD at the D_{2h} and D_{4h} ground-state geometries. Computational details are reported in Section 2. Section 3 is devoted to the discussion of our results. Finally, our conclusions are drawn in Section 4.

2. COMPUTATIONAL DETAILS

2.A. Selected Configuration Interaction Calculations. For the SCI calculations, we rely on the CIPSI algorithm implemented in the QUANTUM PACKAGE,[92] which iteratively selects determinants in the FCI space. To treat electronic states on an equal footing, we use a state-averaged formalism where the ground and excited states are expanded with the same set of determinants but with different CI coefficients. Note that the determinant selection for these states is performed simultaneously via the protocol described in refs 92 and 114.

For a given size of the variational wave function and for each electronic state, the CIPSI energy is the sum of two terms: the variational energy obtained by diagonalization of the CI matrix in the reference space $E_{\text{var.}}$ and a second-order perturbative correction E_{PT2} which estimates the contribution of the external determinants that are not included in the variational space at a given iteration. The sum of these two energies is, for large enough wave functions, an estimate of the FCI energy of a given state, i.e., $E_{\text{FCI}} \approx E_{\text{var.}} + E_{\text{PT2}}$. It is possible to estimate more precisely the FCI energy via an extrapolation procedure, where the variational energy is extrapolated to $E_{\text{PT2}} = 0$.[84] Excitation energies are then computed as differences of extrapolated total energies.[36,60,61,89,90] Additionally, an error bar can be provided thanks to a recent method based on Gaussian random variables that is described in ref 96. This type of extrapolation procedures is now routine in SCI and similar techniques.[91,93,115]

2.B. Coupled-Cluster Calculations. Coupled-cluster theory provides a hierarchy of methods that yields increasingly accurate ground-state energies by ramping up the maximum excitation degree of the cluster operator:[11,116−120] CC with singles and doubles (CCSD),[116,121] CC with singles, doubles, and triples (CCSDT),[122,123] CC with singles, doubles, triples, and quadruples (CCSDTQ),[124−126] etc. As mentioned above, CC theory can be extended to excited states via the EOM formalism,[56,57] where one diagonalizes the similarity-transformed Hamiltonian in a CI basis of excited determinants

https://doi.org/10.1021/acs.jpca.2c02480
J. Phys. Chem. A 2022, 126, 4664−4679

yielding the following systematically improvable family of methods for neutral excited states:[46−49,57,58,122,127−130] EOM-CCSD, EOM-CCSDT, EOM-CCSDTQ, etc. In the following, we will omit the prefix EOM for the sake of conciseness. Alternatively to the "complete" CC models, one can also employ the CC2,[131,132] CC3,[131,133] and CC4[97,134,135] methods which can be seen as cheaper approximations of CCSD, CCSDT, and CCSDTQ by skipping the most expensive terms and avoiding the storage of high-order amplitudes.

Here, we have performed CC calculations using various codes. Typically, CCSD, CCSDT, and CCSDTQ as well as CC3 and CC4 calculations are achieved with CFOUR,[135] with which only singlet excited states can be computed (except for CCSD). In some cases, we have also computed (singlet and triplet) excitation energies and properties (such as the percentage of single excitations involved in a given transition, namely $\%T_1$) at the CC3 level with DALTON[136] and at the CCSDT level with MRCC.[137]

To avoid having to perform multireference CC calculations or high-level CC calculations in the restricted open-shell or unrestricted formalisms, it is worth mentioning that, for the D_{4h} arrangement, we have considered the lowest *closed-shell* singlet state of A_g symmetry as reference. Hence, the open-shell ground state, 1^1B_{1g}, and the 1^1B_{2g} state appear as a de-excitation and an excitation, respectively. With respect to this closed-shell reference, 1^1B_{1g} has a dominant double excitation character, while 1^1B_{2g} has a dominant single excitation character, hence their contrasting convergence behaviors with respect to the order of the CC expansion (see below).

2.C. Multireference Calculations. State-averaged CASSCF (SA-CASSCF) calculations are performed for vertical transition energies, whereas state-specific CASSCF is used for computing the automerization barrier.[138] For each excited state, a set of state-averaged orbitals is computed by taking into account the excited state of interest as well as the ground state (even if it has a different symmetry). Two active spaces have been considered: (i) a minimal (4e,4o) active space including the valence π orbitals and (ii) an extended (12e,12o) active space where we have additionally included the σ_{CC} and σ^*_{CC} orbitals. For ionic excited states, like the 1^1B_{1g} state of CBD, it is particularly important to take into account the $\sigma-\pi$ coupling.[139−141]

On top of this CASSCF treatment, CASPT2 calculations are performed within the RS2 contraction scheme, while the NEVPT2 energies are computed within both the partially contracted (PC) and strongly contracted (SC) schemes.[53−55] Note that PC-NEVPT2 is theoretically more accurate than SC-NEVPT2 due to the larger number of external configurations and greater flexibility. In order to avoid the intruder state problem in CASPT2, a real-valued level shift of 0.3 E_h is set,[10,142] with an additional ionization-potential-electron-affinity (IPEA) shift of 0.25 E_h to avoid systematic underestimation of the vertical excitation energies.[143−146] For the sake of comparison and completeness, for the (4e,4o) active space, we also report (in the Supporting Information) multireference CI calculations including Davidson correction (MRCI+Q).[147,148] All these calculations are carried out with MOLPRO.[138]

2.D. Spin-Flip Calculations. Within the spin-flip formalism, one considers the lowest triplet state as reference instead of the singlet ground state. Ground-state energies are then computed as sums of the triplet reference state energy and the corresponding de-excitation energy. Likewise, excitation energies with respect to the singlet ground state are computed as differences of excitation energies with respect to the reference triplet state.

Nowadays, spin-flip techniques are broadly accessible thanks to intensive developments in the electronic structure community (see ref 103 and references therein). Here, we explore the spin-flip version[149] of the algebraic-diagrammatic construction[150] (ADC) using the standard and extended second-order ADC schemes, SF-ADC(2)-s[18,151] and SF-ADC(2)-x,[18] as well as its third-order version, SF-ADC(3).[18,152,153] These calculations are performed using Q-CHEM 5.4.1.[154] The spin-flip version of our recently proposed composite approach, namely SF-ADC(2.5),[155] where one simply averages the SF-ADC(2)-s and SF-ADC(3) energies, is also tested in the following.

We have also carried out spin-flip calculations within the TD-DFT framework (SF-TD-DFT).[156] The B3LYP,[157−159] PBE0,[160,161] and BH&HLYP global hybrid GGA functionals are considered, which contain 20%, 25%, and 50% of exact exchange, respectively. These calculations are labeled as SF-TD-B3LYP, SF-TD-PBE0, and SF-TD-BH&HLYP in the following. Additionally, we have also computed SF-TD-DFT excitation energies using range-separated hybrid (RSH) functionals: CAM-B3LYP (19% of short-range exact exchange and 65% at long-range),[162] LC-ωPBE08 (0% of short-range exact exchange and 100% at long-range),[163] and ωB97X-V (16.7% of short-range exact exchange and 100% at long-range).[164] Finally, the hybrid meta-GGA functional M06-2X (54% of exact exchange)[165] and the RSH meta-GGA functional M11 (42.8% of short-range exact exchange and 100% at long-range)[166] are also employed. Note that all SF-TD-DFT calculations are done within the Tamm-Dancoff approximation.[167]

There also exist spin-flip extensions of EOM-CC methods,[100,168−171] and we consider here the spin-flip version of EOM-CCSD, named SF-EOM-CCSD.[100] Additionally, Manohar and Krylov introduced a noniterative triples correction to EOM-CCSD and extended it to the spin-flip variant.[169] Two types of triples corrections were proposed: (i) EOM-CCSD-(dT) that uses the diagonal elements of the similarity-transformed CCSD Hamiltonian and (ii) EOM-CCSD(fT) where the Hartree−Fock orbital energies are considered instead.

All spin-flip calculations have been performed with Q-CHEM 5.4.1.[154] Note that symmetry labels may vary as different packages use different standard orientations. Here, we have consistently followed the so-called Mulliken conventions.[172]

2.E. Theoretical Best Estimates. When technically possible, each level of theory is tested with four Gaussian basis sets, namely, 6-31+G(d) and aug-cc-pVXZ with X = D, T, and Q.[173] This helps us to assess the convergence of each property with respect to the size of the basis set. More importantly, for each studied quantity (i.e., the automerization barrier and the vertical excitation energies), we provide a theoretical best estimate (TBE) established in the aug-cc-pVTZ basis. These TBEs are defined using extrapolated CCSDTQ/aug-cc-pVTZ values except in a single occasion where the NEVPT2(12,12) value is used.

The extrapolation of the CCSDTQ/aug-cc-pVTZ values is done via a "pyramidal" scheme, where we employ systematically the most accurate level of theory and the largest basis set available. The viability of this scheme lies on the transferability of basis set effects within wave function methods (see below). For example, when CC4/aug-cc-pVTZ and CCSDTQ/aug-cc-pVDZ data are available, we proceed via the following basis set extrapolation:

https://doi.org/10.1021/acs.jpca.2c02480
J. Phys. Chem. A 2022, 126, 4664−4679

$$\Delta\tilde{E}^{\mathrm{CCSDTQ}}_{\text{aug-cc-pVTZ}} = \Delta E^{\mathrm{CCSDTQ}}_{\text{aug-cc-pVDZ}} + \left[\Delta E^{\mathrm{CC4}}_{\text{aug-cc-pVTZ}} - \Delta E^{\mathrm{CC4}}_{\text{aug-cc-pVDZ}}\right] \quad (1)$$

while, when only CCSDTQ/6-31G+(d) values are available, we further extrapolate the CCSDTQ/aug-cc-pVDZ value as follows:

$$\Delta\tilde{E}^{\mathrm{CCSDTQ}}_{\text{aug-cc-pVDZ}} = \Delta E^{\mathrm{CCSDTQ}}_{\text{6-31G+(d)}} + \left[\Delta E^{\mathrm{CC4}}_{\text{aug-cc-pVDZ}} - \Delta E^{\mathrm{CC4}}_{\text{6-31G+(d)}}\right] \quad (2)$$

If we lack the CC4 data, we can follow the same philosophy and rely on CCSDT (for single excitations) or NEVPT2 (for double excitations). For example,

$$\Delta\tilde{E}^{\mathrm{CC4}}_{\text{aug-cc-pVTZ}} = \Delta E^{\mathrm{CC4}}_{\text{aug-cc-pVDZ}} + \left[\Delta E^{\mathrm{CCSDT}}_{\text{aug-cc-pVTZ}} - \Delta E^{\mathrm{CCSDT}}_{\text{aug-cc-pVDZ}}\right] \quad (3)$$

and so on. If neither CC4 nor CCSDT is feasible, then we rely on PC-NEVPT2(12,12). The procedures applied for each extrapolated value are explicitly mentioned as footnotes in the tables. Note that, due to the error bar inherently linked to the CIPSI calculations (see Section 2.A), these are mostly used as an additional safety net to further check the convergence of the CCSDTQ estimates.

Additional tables gathering these TBEs as well as literature data for the autoerization barrier and the vertical excitation energies can be found in the Supporting Information.

3. RESULTS AND DISCUSSION

3.A. Geometries. Two different sets of geometries obtained with different levels of theory are considered for the automerization barrier and the excited states of the CBD molecule. First, because the automerization barrier is obtained as a difference of energies computed at distinct geometries, it is paramount to obtain these at the same level of theory. However, due to the fact that the ground state of the square arrangement is a transition state of singlet open-shell nature, it is technically difficult to optimize the geometry with high-order CC methods. Therefore, we rely on CASPT2(12,12)/aug-cc-pVTZ for both the D_{2h} and D_{4h} ground-state structures. (Note that these optimizations are done without the IPEA shift but with a level shift and a state-specific reference CASSCF wave function.) Second, because the vertical transition energies are computed for a particular equilibrium geometry, we can afford to use different methods for the rectangular and square structures. Hence, we rely on CC3/aug-cc-pVTZ to compute the equilibrium geometry of the 1^1A_g state in the rectangular (D_{2h}) arrangement and the restricted open-shell (RO) version of CCSD(T)/aug-cc-pVTZ to obtain the equilibrium geometry of the 1^3A_{2g} state in the square (D_{4h}) arrangement. These two geometries are the lowest-energy equilibrium structure of their respective spin manifold (see Figure 1). The Cartesian coordinates of these geometries are provided in the Supporting Information. Table 1 reports the key geometrical parameters obtained at these levels of theory as well as previous geometries computed by Manohar and Krylov at the CCSD(T)/cc-pVTZ level. One notes the globally satisfying agreement between the tested methods with variations of the order of 0.01 Å only.

Table 1. Optimized Geometries Associated with Several States of CBD Computed with Various Levels of Theory[c]

state	method	C=C	C−C	C−H	∠H−C=C
D_{2h} (1^1A_g)	CASPT2(12,12)/aug-cc-pVTZ[a]	1.354	1.566	1.077	134.99
	CC3/aug-cc-pVTZ[a]	1.344	1.565	1.076	135.08
	CCSD(T)/cc-pVTZ[b]	1.343	1.566	1.074	135.09
D_{4h} (1^1B_{1g})	CASPT2(12,12)/aug-cc-pVTZ[a]	1.449	1.449	1.076	135.00
D_{4h} (1^3A_{2g})	CASPT2(12,12)/aug-cc-pVTZ[a]	1.445	1.445	1.076	135.00
	RO-CCSD(T)/aug-cc-pVTZ[a]	1.439	1.439	1.075	135.00
	RO-CCSD(T)/cc-pVTZ[b]	1.439	1.439	1.073	135.00

[a]This work. [b]From ref 169. [c]Bond lengths are in Å, and angles (∠) are in degrees.

Table 2. Autoerization Barrier (in kcal mol^{-1}) of CBD Computed with Various Computational Methods and Basis Sets[g]

	basis sets			
method	6-31+G(d)	aug-cc-pVDZ	aug-cc-pVTZ	aug-cc-pVQZ
SF-TD-B3LYP	18.59	18.64	19.34	19.34
SF-TD-PBE0	17.18	17.19	17.88	17.88
SF-TD-BH&HLYP	11.90	12.02	12.72	12.73
SF-TD-M06-2X	9.32	9.62	10.35	10.37
SF-TD-CAM-B3LYP	18.05	18.10	18.83	18.83
SF-TD-ωB97X-V	18.26	18.24	18.94	18.92
SF-TD-LC-ωPBE08	19.05	18.98	19.74	19.71
SF-TD-M11	11.03	10.25	11.22	11.12
SF-ADC(2)-s	6.69	6.98	8.63	
SF-ADC(2)-x	8.63	8.96	10.37	
SF-ADC(2.5)	7.36	7.76	9.11	
SF-ADC(3)	8.03	8.54	9.58	
SF-EOM-CCSD	5.86	6.27	7.40	
CASSCF(4,4)	6.17	6.59	7.38	7.41
CASPT2(4,4)	6.56	6.87	7.77	7.93
SC-NEVPT2(4,4)	7.95	8.31	9.23	9.42
PC-NEVPT2(4,4)	7.95	8.33	9.24	9.41
CASSCF(12,12)	10.19	10.75	11.59	11.62
CASPT2(12,12)	7.24	7.53	8.51	8.71
SC-NEVPT2(12,12)	7.10	7.32	8.29	8.51
PC-NEVPT2(12,12)	7.12	7.33	8.28	8.49
CCSD	8.31	8.80	9.88	10.10
CC3	6.59	6.89	7.88	8.06
CCSDT	7.26	7.64	8.68	[8.86][a]
CC4	7.40	7.78	[8.82][b]	[9.00][c]
CCSDTQ	7.51	[7.89][d]	[**8.93**][e]	[9.11][f]

[a]Value obtained using CCSDT/aug-cc-pVTZ corrected by the difference between CC3/aug-cc-pVQZ and CC3/aug-cc-pVTZ. [b]Value obtained using CC4/aug-cc-pVDZ corrected by the difference between CCSDT/aug-cc-pVTZ and CCSDT/aug-cc-pVDZ. [c]Value obtained using CC4/aug-cc-pVTZ corrected by the difference between CCSDT/aug-cc-pVQZ and CCSDT/aug-cc-pVTZ. [d]Value obtained using CCSDTQ/6-31+G(d) corrected by the difference between CC4/aug-cc-pVDZ basis and CC4/6-31+G(d). [e]TBE value obtained using CCSDTQ/aug-cc-pVDZ corrected by the difference between CC4/aug-cc-pVTZ and CC4/aug-cc-pVDZ. [f]Value obtained using CCSDTQ/aug-cc-pVTZ corrected by the difference between CC4/aug-cc-pVQZ and CC4/aug-cc-pVTZ. [g]The values in square parentheses have been obtained by extrapolation via the procedure described in the corresponding footnote. The TBE/aug-cc-pVTZ value is highlighted in bold.

3.B. Automerization Barrier. The results concerning the automerization barrier are reported in Table 2 for various basis sets and shown in Figure 2 for the aug-cc-pVTZ basis. Our TBE with this basis set is 8.93 kcal mol^{-1}, which is in excellent

https://doi.org/10.1021/acs.jpca.2c02480
J. Phys. Chem. A 2022, 126, 4664−4679

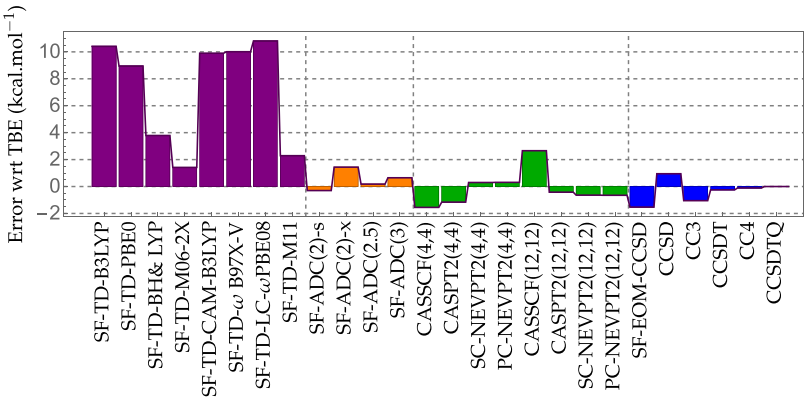

Figure 2. Error (with respect to the TBE) in the automerization barrier (in kcal mol^{-1}) of CBD at various levels of theory using the aug-cc-pVTZ basis. See the Supporting Information for the total energies.

agreement with previous studies[32−35,174,175] (see the Supporting Information).

First, one can see large variations of the energy barrier at the SF-TD-DFT level, with differences as large as 10 kcal mol^{-1} between the different functionals for a given basis set. Nonetheless, it is clear that the performance of a given functional is directly linked to the amount of exact exchange at short-range. Indeed, hybrid functionals with approximately 50% of short-range exact exchange (e.g., BH&HLYP, M06-2X, and M11) perform significantly better than the functionals having a small fraction of short-range exact exchange (e.g., B3LYP, PBE0, CAM-B3LYP, ωB97X-V, and LC-ωPBE08). However, they are still off by 1−4 kcal mol^{-1} from the TBE reference value, the most accurate result being obtained with M06-2X. For the RSH functionals, the automerization barrier is much less sensitive to the amount of long-range exact exchange. Another important feature of SF-TD-DFT is the fast convergence of the energy barrier with the size of the basis set.[176] With the augmented double-ζ basis, the SF-TD-DFT results are basically converged to subkcal mol^{-1} accuracy, which is a drastic improvement compared to wave function approaches where this type of convergence is reached with the augmented triple-ζ basis only.

For the SF-ADC family of methods, the energy differences are much smaller with a maximum deviation of 2 kcal mol^{-1} between different versions. In particular, we observe that SF-ADC(2)-s and SF-ADC(3), which respectively scale as $O(N^5)$ and $O(N^6)$ (where N is the number of basis functions), under- and overestimate the automerization barrier, making SF-ADC(2.5) a good compromise with an error of only 0.18 kcal mol^{-1} compared to the TBE/aug-cc-pVTZ reference value. Nonetheless, at a $O(N^5)$ computational scaling, SF-ADC(2)-s is particularly accurate, even compared to high-order CC methods (see below). We note that SF-ADC(2)-x [which scales as $O(N^6)$] is probably not worth its extra cost [as compared to SF-ADC(2)-s] as it overestimates the energy barrier even more than SF-ADC(3). This behavior was previously reported by Dreuw's group.[18,153,177] Overall, even with the best exchange-correlation functional, SF-TD-DFT is clearly outperformed by the more expensive SF-ADC models.

We observe that SF-EOM-CCSD/aug-cc-pVTZ tends to underestimate by about 1.5 kcal mol^{-1} the energy barrier compared to the TBE, an observation in agreement with previous results by Manohar and Krylov.[169] This can be alleviated by including the triples correction with SF-EOM-CCSD(fT) and SF-EOM-CCSD(dT) (see the Supporting Information where we have reported the data from ref 169). We also note that the SF-EOM-CCSD values for the energy barrier are close to the ones obtained with the more expensive (standard) CC3 method yet less accurate than values computed with the cheaper SF-ADC(2)-s formalism. Note that, in contrast to a previous statement,[169] the (fT) correction performs better than the (dT) correction for the energy barrier. However, for the excited states, the situation is reversed (see below).

Concerning the multireference approaches with the minimal (4e,4o) active space, the TBEs are bracketed by the CASPT2 and NEVPT2 values that differ by approximately 1.5 kcal mol^{-1} for all bases. In this case, the NEVPT2 values are fairly accurate with differences below half a kcal mol^{-1} compared to the TBEs. The CASSCF results predict an even lower barrier than CASPT2 due to the well-known lack of dynamical correlation at the CASSCF level. For the larger (12e,12o) active space, we see larger differences of the order of 3 kcal mol^{-1} (through all the bases) between CASSCF and the second-order variants (CASPT2 and NEVPT2). However, the deviations between CASPT2(12,12) and NEVPT2(12,12) are much smaller than with the minimal active space, with an energy difference of around 0.1−0.2 kcal mol^{-1} for all bases and CASPT2 being slightly more accurate than NEVPT2 in this case. For each basis set, both CASPT2(12,12) and NEVPT2(12,12) are less than a kcal mol^{-1} away from the TBEs. For the two active spaces that we have considered here, the PC- and SC-NEVPT2 schemes provide nearly identical barriers independently of the size of the one-electron basis.

Finally, for the CC family of methods, we observe the usual systematic improvement following the series CCSD < CC3 < CCSDT < CC4 < CCSDTQ, which parallels their increase in computational cost: $O(N^6)$, $O(N^7)$, $O(N^8)$, $O(N^9)$, and $O(N^{10})$, respectively. Note that the introduction of the triple excitations is clearly mandatory to have an accuracy beyond SF-TD-DFT, and we observe that CCSDT is definitely an improvement over its cheaper, approximated version, CC3.

3.C. Vertical Excitation Energies. *3.C.1. D_{2h} Rectangular Geometry.* Table 3 reports, at the D_{2h} rectangular equilibrium geometry of the 1^1A_g ground state, the vertical transition energies associated with the 1^3B_{1g}, 1^1B_{1g}, and 2^1A_g states obtained using the spin-flip formalism, while Table 4 gathers the same quantities obtained with the multireference, CC, and CIPSI methods. Considering the aug-cc-pVTZ basis, the

https://doi.org/10.1021/acs.jpca.2c02480
J. Phys. Chem. A 2022, 126, 4664−4679

Table 3. Spin-Flip TD-DFT and ADC Vertical Excitation Energies (with Respect to the Singlet 1^1A_g Ground State) of the 1^3B_{1g}, 1^1B_{1g}, and 2^1A_g States of CBD at the D_{2h} Rectangular Equilibrium Geometry of the 1^1A_g Ground State

		excitation energies (eV)		
method	basis	1^3B_{1g}	1^1B_{1g}	2^1A_g
SF-TD-B3LYP	6-31+G(d)	1.706	2.211	3.993
	aug-cc-pVDZ	1.706	2.204	3.992
	aug-cc-pVTZ	1.703	2.199	3.988
	aug-cc-pVQZ	1.703	2.199	3.989
SF-TD-PBE0	6-31+G(d)	1.687	2.314	4.089
	aug-cc-pVDZ	1.684	2.301	4.085
	aug-cc-pVTZ	1.682	2.296	4.081
	aug-cc-pVQZ	1.682	2.296	4.079
SF-TD-BH&HLYP	6-31+G(d)	1.552	2.779	4.428
	aug-cc-pVDZ	1.546	2.744	4.422
	aug-cc-pVTZ	1.540	2.732	4.492
	aug-cc-pVQZ	1.540	2.732	4.415
SF-TD-M06-2X	6-31+G(d)	1.477	2.835	4.378
	aug-cc-pVDZ	1.467	2.785	4.360
	aug-cc-pVTZ	1.462	2.771	4.357
	aug-cc-pVQZ	1.458	2.771	4.352
SF-TD-CAM-B3LYP	6-31+G(d)	1.750	2.337	4.140
	aug-cc-pVDZ	1.745	2.323	4.140
	aug-cc-pVTZ	1.742	2.318	4.138
	aug-cc-pVQZ	1.743	2.319	4.138
SF-TD-ωB97X-V	6-31+G(d)	1.810	2.377	4.220
	aug-cc-pVDZ	1.800	2.356	4.217
	aug-cc-pVTZ	1.797	2.351	4.213
	aug-cc-pVQZ	1.797	2.351	4.213
SF-TD-LC-ωPBE08	6-31+G(d)	1.917	2.445	4.353
	aug-cc-pVDZ	1.897	2.415	4.346
	aug-cc-pVTZ	1.897	2.415	4.348
	aug-cc-pVQZ	1.897	2.415	4.348
SF-TD-M11	6-31+G(d)	1.566	2.687	4.292
	aug-cc-pVDZ	1.546	2.640	4.267
	aug-cc-pVTZ	1.559	2.651	4.300
	aug-cc-pVQZ	1.557	2.650	4.299
SF-ADC(2)-s	6-31+G(d)	1.577	3.303	4.196
	aug-cc-pVDZ	1.513	3.116	4.114
	aug-cc-pVTZ	1.531	3.099	4.131
	aug-cc-pVQZ	1.544	3.101	4.140
SF-ADC(2)-x	6-31+G(d)	1.557	3.232	3.728
	aug-cc-pVDZ	1.524	3.039	3.681
	aug-cc-pVTZ	1.539	3.031	3.703
SF-ADC(2.5)	6-31+G(d)	1.496	3.328	4.219
	aug-cc-pVDZ	1.468	3.148	4.161
	aug-cc-pVTZ	1.475	3.131	4.178
SF-ADC(3)	6-31+G(d)	1.435	3.352	4.242
	aug-cc-pVDZ	1.422	3.180	4.208
	aug-cc-pVTZ	1.419	3.162	4.224
SF-EOM-CCSD	6-31+G(d)	1.663	3.515	4.275
	aug-cc-pVDZ	1.611	3.315	4.216
	aug-cc-pVTZ	1.609	3.293	4.245

evolution of the vertical excitation energies with respect to the level of theory is illustrated in Figure 3.

At the CC3/aug-cc-pVTZ level, the percentage of single excitation involved in the 1^3B_{1g}, 1^1B_{1g}, and 2^1A_g is 99%, 95%, and 1%, respectively. Therefore, the two formers are dominated by single excitations, while the latter state corresponds to a genuine double excitation.

First, let us discuss basis set effects at the SF-TD-DFT level (Table 3). As expected, these are found to be small, and the results are basically converged to the complete basis set limit with the triple-ζ basis, which is definitely not the case for the wave function methods.[178] Regarding now the accuracy of the vertical excitation energies, again, we see that, for 1^3B_{1g} and 1^1B_{1g}, the functionals with the largest amount of short-range exact exchange (e.g., BH&HLYP, M06-2X, and M11) are the most accurate. Functionals with a large share of exact exchange are known to perform best in the SF-TD-DFT framework as the Hartree−Fock exchange term is the only nonvanishing term in the spin-flip block.[156] However, their overall accuracy remains average especially for the singlet states, 1^1B_{1g} and 2^1A_g, with an error of the order of 0.2−0.5 eV compared to the TBEs. The triplet state, 1^3B_{1g}, is much better described with errors below 0.1 eV. Surprisingly, for the doubly excited state, 2^1A_g, the hybrid functionals with a low percentage of exact exchange (B3LYP and PBE0) are the best performers with absolute errors below 0.05 eV. Note that, as evidenced by the data reported in Supporting Information, none of these states exhibit a strong spin contamination.

Second, we discuss the various SF-ADC schemes (Table 3), i.e., SF-ADC(2)-s, SF-ADC(2)-x, and SF-ADC(3). At the SF-ADC(2)-s level, going from the smallest 6-31+G(d) basis to the largest aug-cc-pVQZ basis induces a small decrease in vertical excitation energies of 0.03 eV (0.06 eV) for the 1^3B_{1g} (2^1A_g) state, while the transition energy of the 1^1B_{1g} state drops more significantly by about 0.2 eV. [The SF-ADC(2)-x and SF-ADC(3) calculations with aug-cc-pVQZ were not feasible with our computational resources.] These basis set effects are fairly transferable to the other wave function methods that we have considered here. This further motivates the "pyramidal" extrapolation scheme that we have employed to produce the TBE values (see Section 2.E). Again, the extended version, SF-ADC(2)-x, does not seem to be relevant in the present context with much larger errors than the other schemes. Also, as reported previously,[155] SF-ADC(2)-s and SF-ADC(3) have mirror error patterns making SF-ADC(2.5) particularly accurate except for the doubly excited state 2^1A_g where the error with respect to the TBE (0.140 eV) is larger than the SF-ADC(2)-s error (0.093 eV).

Interestingly, we observe that the SF-EOM-CCSD excitation energies are systematically larger than the TBEs by approximately 0.2 eV with a nice consistency throughout the various (singly- and doubly-) excited states. Moreover, SF-EOM-CCSD excitation energies are somehow closer to their SF-ADC(2)-s analogs (with an energy difference of about 0.1 eV) than the other schemes as already noticed by LeFrançois and coworkers.[149] We see that the SF-EOM-CCSD excitation energies for the triplet state are larger by about 0.3 eV compared to the CCSD ones, which was also pointed out in the study of Manohar and Krylov.[169] Again, our SF-EOM-CCSD results are very similar to the ones obtained in previous studies.[149,169] We can logically expect a similar trend for SF-EOM-CCSD(fT) and SF-EOM-CCSD(dT) that lower the excitation energies and tend to be in better agreement with respect to the TBE (see the Supporting Information). Note that the (dT) correction slightly outperforms the (fT) correction as previously observed[169] and theoretically expected.

Let us now move to the discussion of the results obtained with standard wave function methods that are reported in Table 4. Regarding the multireference calculations, the most striking result is the poor description of the 1^1B_{1g} ionic state, especially

https://doi.org/10.1021/acs.jpca.2c02480
J. Phys. Chem. A 2022, 126, 4664−4679

Table 4. Vertical Excitation Energies (with Respect to the 1^1A_g Ground State) of the 1^3B_{1g}, 1^1B_{1g}, and 2^1A_g States of CBD at the D_{2h} Rectangular Equilibrium Geometry of the 1^1A_g Ground State[g]

		excitation energies (eV)		
method	basis	1^3B_{1g}	1^1B_{1g}	2^1A_g
CASSCF(4,4)	6-31+G(d)	1.662	4.657	4.439
	aug-cc-pVDZ	1.672	4.563	4.448
	aug-cc-pVTZ	1.670	4.546	4.441
	aug-cc-pVQZ	1.671	4.549	4.440
CASPT2(4,4)	6-31+G(d)	1.440	3.162	4.115
	aug-cc-pVDZ	1.414	2.971	4.068
	aug-cc-pVTZ	1.412	2.923	4.072
	aug-cc-pVQZ	1.417	2.911	4.081
SC-NEVPT2(4,4)	6-31+G(d)	1.407	2.707	4.145
	aug-cc-pVDZ	1.381	2.479	4.109
	aug-cc-pVTZ	1.379	2.422	4.108
	aug-cc-pVQZ	1.384	2.408	4.116
PC-NEVPT2(4,4)	6-31+G(d)	1.409	2.652	4.120
	aug-cc-pVDZ	1.384	2.424	4.084
	aug-cc-pVTZ	1.382	2.368	4.083
	aug-cc-pVQZ	1.387	2.353	4.091
CASSCF(12,12)	6-31+G(d)	1.675	3.924	4.220
	aug-cc-pVDZ	1.685	3.856	4.221
	aug-cc-pVTZ	1.686	3.844	4.217
	aug-cc-pVQZ	1.687	3.846	4.216
CASPT2(12,12)	6-31+G(d)	1.508	3.407	4.099
	aug-cc-pVDZ	1.489	3.256	4.044
	aug-cc-pVTZ	1.480	3.183	4.043
	aug-cc-pVQZ	1.482	3.163	4.047
SC-NEVPT2(12,12)	6-31+G(d)	1.522	3.409	4.130
	aug-cc-pVDZ	1.511	3.266	4.093
	aug-cc-pVTZ	1.501	3.188	4.086
	aug-cc-pVQZ	1.503	3.167	4.088
PC-NEVPT2(12,12)	6-31+G(d)	1.487	3.296	4.103
	aug-cc-pVDZ	1.472	3.141	4.064
	aug-cc-pVTZ	1.462	3.063	4.056
	aug-cc-pVQZ	1.464	3.043	4.059
CCSD	6-31+G(d)	1.346	3.422	
	aug-cc-pVDZ	1.319	3.226	
	aug-cc-pVTZ	1.317	3.192	
	aug-cc-pVQZ	1.323	3.187	
CC3	6-31+G(d)	1.420	3.341	4.658
	aug-cc-pVDZ	1.396	3.158	4.711
	aug-cc-pVTZ	1.402	3.119	4.777
	aug-cc-pVQZ	1.409	3.113	4.774
CCSDT	6-31+G(d)	1.442	3.357	4.311
	aug-cc-pVDZ	1.411	3.175	4.327
	aug-cc-pVTZ	1.411	3.139	4.429
CC4	6-31+G(d)		3.343	4.067
	aug-cc-pVDZ		3.164	4.040
	aug-cc-pVTZ		[3.128][a]	[4.032][b]
CCSDTQ	6-31+G(d)	1.464	3.340	4.073
	aug-cc-pVDZ	[1.433][c]	[3.161][d]	[4.046][d]
	aug-cc-pVTZ	[**1.433**][e]	[**3.125**][f]	[**4.038**][f]
CIPSI	6-31+G(d)	1.486 ± 0.005	3.348 ± 0.024	4.084 ± 0.012
	aug-cc-pVDZ	1.458 ± 0.009	3.187 ± 0.035	4.04 ± 0.04
	aug-cc-pVTZ	1.461 ± 0.030	3.142 ± 0.035	4.03 ± 0.09

[a]Value obtained using CC4/aug-cc-pVDZ corrected by the difference between CCSDT/aug-cc-pVTZ and CCSDT/aug-cc-pVDZ. [b]Value obtained using CC4/aug-cc-pVDZ corrected by the difference between PC-NEVPT2(12,12)/aug-cc-pVTZ and PC-NEVPT2(12,12)/aug-cc-pVDZ. [c]Value obtained using CCSDTQ/6-31+G(d) corrected by the difference between CCSDT/aug-cc-pVDZ and CCSDT/6-31+G(d). [d]Value obtained using CCSDTQ/6-31+G(d) corrected by the difference between CC4/aug-cc-pVDZ and CC4/6-31+G(d). [e]Value obtained using CCSDTQ/aug-cc-pVDZ corrected by the difference between CCSDT/aug-cc-pVTZ and CCSDT/aug-cc-pVDZ. [f]TBE value obtained using CCSDTQ/aug-cc-pVDZ corrected by the difference between CC4/aug-cc-pVTZ and CC4/aug-cc-pVDZ. [g]The values in square parentheses have been obtained by extrapolation via the procedure described in the corresponding footnote. The TBE/aug-cc-pVTZ values are highlighted in bold.

https://doi.org/10.1021/acs.jpca.2c02480
J. Phys. Chem. A 2022, 126, 4664−4679

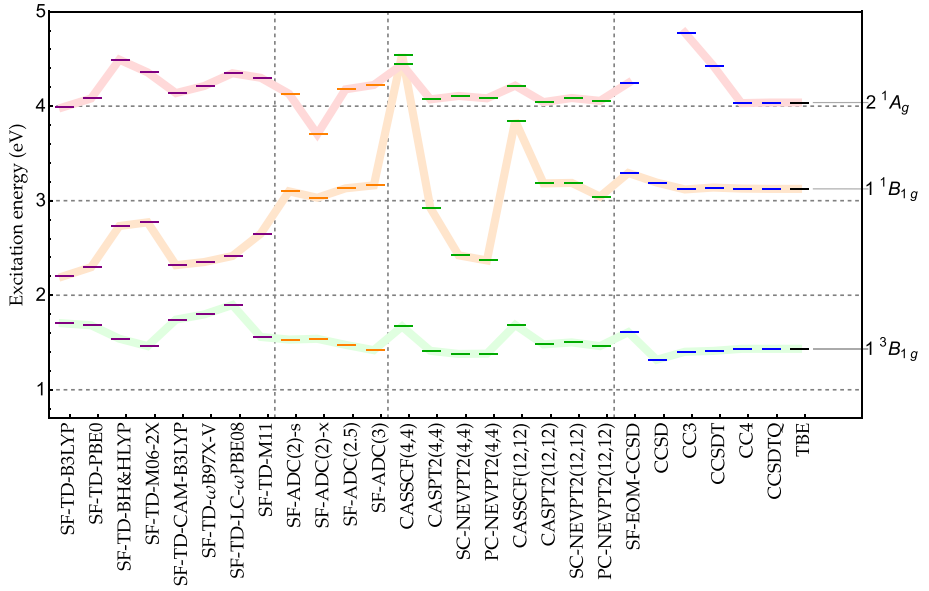

Figure 3. Vertical excitation energies of the 1^3B_{1g}, 1^1B_{1g}, and 2^1A_g states at the D_{2h} rectangular equilibrium geometry of the 1^1A_g ground state using the aug-cc-pVTZ basis. See the Supporting Information for the raw data.

with the (4e,4o) active space where CASSCF predicts this state higher in energy than the 2^1A_g state. Of course, the PT2 correction is able to correct the state ordering problem but cannot provide quantitative excitation energies due to the poor zeroth-order treatment. Another ripple effect of the unreliability of the reference wave function is the large difference between CASPT2 and NEVPT2 that differ by half an eV. This feature is characteristic of the inadequacy of the active space to model such a state. Additional MRCI and MRCI+Q calculations (reported in the Supporting Information) confirm this. For the two other states, 1^3B_{1g} and 2^1A_g, the errors at the CASPT2(4,4) and NEVPT2(4,4) levels are much smaller (below 0.1 eV). Using a larger active space resolves most of these issues: CASSCF predicts the correct state ordering (though the ionic state is still badly described in term of energetics), CASPT2 and NEVPT2 excitation energies are much closer, and their accuracy is often improved (especially for the triplet and doubly excited states) although it is difficult to reach chemical accuracy (i.e., an error below 0.043 eV) on a systematic basis.

Finally, for the CC models (Table 4), the two states with a large $\%T_1$ value, 1^3B_{1g} and 1^1B_{1g}, are already extremely accurate at the CC3 level and systematically improved by CCSDT and CC4. This trend is in line with the observations made on the QUEST database.[96] For the doubly excited state, 2^1A_g, the convergence of the CC expansion is much slower, but it is worth pointing out that the inclusion of approximate quadruples via CC4 is particularly effective, as observed in an earlier work.[97] The CCSDTQ excitation energies (which are used to define the TBEs) are systematically within the error bar of the CIPSI extrapolations, which confirms the outstanding performance of CC methods that include quadruple excitations in the context of excited states.

3.C.2. D_{4h} Square-Planar Geometry. In Table 5, we report, at the D_{4h} square-planar equilibrium geometry of the 1^3A_{2g} state, the vertical transition energies associated with the 1^3A_{2g}, 1^1A_{1g}, and 1^1B_{2g} states obtained using the spin-flip formalism, while Table 6 gathers the same quantities obtained with the multireference, CC, and CIPSI methods. The vertical excitation energies computed at various levels of theory are depicted in Figure 4 for the aug-cc-pVTZ basis. Unfortunately, due to technical limitations, we could not compute $\%T_1$ values associated with the 1^3A_{2g}, 1^1A_{1g}, and 1^1B_{2g} excited states in the D_{4h} symmetry. However, it is clear from the inspection of the wave function that, with respect to the 1^1B_{1g} ground state, 1^3A_{2g} and 1^1B_{2g} are dominated by single excitations, while 1^1A_{1g} has a strong double excitation character.

As for the previous geometry, we start by discussing the SF-TD-DFT results (Table 5) and, in particular, the singlet−triplet gap, i.e., the energy difference between 1^1B_{1g} and 1^3A_{2g}. For all functionals, this gap is small (basically below 0.1 eV while the TBE value is 0.144 eV), but it is worth mentioning that B3LYP and PBE0 incorrectly deliver a negative singlet−triplet gap (hence a triplet ground state at this geometry). Increasing the fraction of exact exchange in hybrids or relying on RSHs (even with a small amount of short-range exact exchange) allows the recovery of a positive gap and a singlet ground state. At the SF-TD-DFT level, the energy gap between the two singlet excited states, 1^1A_{1g} and 1^1B_{2g}, is particularly small and grows moderately with the amount of exact exchange at short-range. The influence of the exact exchange on the singlet energies is quite significant with an energy difference of the order of 1 eV between the functional with the smallest amount of exact exchange (B3LYP) and the functional with the largest amount (M06-2X). As for the excitation energies computed on the D_{2h} ground-state equilibrium structure and the automerization barrier, the functionals with a large fraction of short-range exact exchange yield more accurate results. Yet, the transition energy to 1^1B_{2g} is off by half an eV compared to the TBE for BH&HLYP and M11, while the doubly excited state is much closer to the reference value (errors of −0.251 and −0.312 eV for BH&HLYP and M11, respectively). With errors of −0.066, −0.097, and −0.247 eV for 1^3A_{2g}, 1^1A_{1g}, and 1^1B_{2g}, M06-2X is the best performer here. Again, for all the excited states, the basis set effects are extremely small at the SF-TD-DFT level. We emphasize that the $\langle S^2 \rangle$ values reported in the Supporting Information indicate again that there is no significant spin contamination in these excited states.

https://doi.org/10.1021/acs.jpca.2c02480
J. Phys. Chem. A 2022, 126, 4664−4679

Table 5. Spin-Flip TD-DFT and ADC Vertical Excitation Energies (with Respect to the Singlet 1^1B_{1g} Ground State) of the 1^3A_{2g}, 1^1A_{1g}, and 1^1B_{2g} States of CBD at the D_{4h} Square-Planar Equilibrium Geometry of the 1^3A_{2g} State

		excitation energies (eV)		
method	basis	1^3A_{2g}	1^1A_{1g}	1^1B_{2g}
SF-TD-B3LYP	6-31+G(d)	−0.016	0.487	0.542
	aug-cc-pVDZ	−0.019	0.477	0.536
	aug-cc-pVTZ	−0.020	0.472	0.533
	aug-cc-pVQZ	−0.020	0.473	0.533
SF-TD-PBE0	6-31+G(d)	−0.012	0.618	0.689
	aug-cc-pVDZ	−0.016	0.602	0.680
	aug-cc-pVTZ	−0.019	0.597	0.677
	aug-cc-pVQZ	−0.018	0.597	0.677
SF-TD-BH&HLYP	6-31+G(d)	0.064	1.305	1.458
	aug-cc-pVDZ	0.051	1.260	1.437
	aug-cc-pVTZ	0.045	1.249	1.431
	aug-cc-pVQZ	0.046	1.250	1.432
SF-TD-M06-2X	6-31+G(d)	0.102	1.476	1.640
	aug-cc-pVDZ	0.086	1.419	1.611
	aug-cc-pVTZ	0.078	1.403	1.602
	aug-cc-pVQZ	0.079	1.408	1.607
SF-TD-CAM-B3LYP	6-31+G(d)	0.021	0.603	0.672
	aug-cc-pVDZ	0.012	0.585	0.666
	aug-cc-pVTZ	0.010	0.580	0.664
	aug-cc-pVQZ	0.010	0.580	0.664
SF-TD-ωB97X-V	6-31+G(d)	0.040	0.600	0.670
	aug-cc-pVDZ	0.029	0.576	0.664
	aug-cc-pVTZ	0.026	0.572	0.662
	aug-cc-pVQZ	0.026	0.572	0.662
SF-TD-LC-ωPBE08	6-31+G(d)	0.078	0.593	0.663
	aug-cc-pVDZ	0.060	0.563	0.659
	aug-cc-pVTZ	0.058	0.561	0.658
	aug-cc-pVQZ	0.058	0.561	0.659
SF-TD-M11	6-31+G(d)	0.102	1.236	1.374
	aug-cc-pVDZ	0.087	1.196	1.362
	aug-cc-pVTZ	0.081	1.188	1.359
	aug-cc-pVQZ	0.080	1.185	1.357
SF-ADC(2)-s	6-31+G(d)	0.345	1.760	2.096
	aug-cc-pVDZ	0.269	1.656	1.894
	aug-cc-pVTZ	0.256	1.612	1.844
SF-ADC(2)-x	6-31+G(d)	0.264	1.181	1.972
	aug-cc-pVDZ	0.216	1.107	1.760
	aug-cc-pVTZ	0.212	1.091	1.731
SF-ADC(2.5)	6-31+G(d)	0.234	1.705	2.087
	aug-cc-pVDZ	0.179	1.614	1.886
	aug-cc-pVTZ	0.168	1.594	1.849
SF-ADC(3)	6-31+G(d)	0.123	1.650	2.078
	aug-cc-pVDZ	0.088	1.571	1.878
	aug-cc-pVTZ	0.079	1.575	1.853
SF-EOM-CCSD	6-31+G(d)	0.446	1.875	2.326
	aug-cc-pVDZ	0.375	1.776	2.102
	aug-cc-pVTZ	0.354	1.768	2.060

Next, we discuss the various ADC schemes (Table 5). Globally, we observe similar trends as those noted in Section 3.C.1. Concerning the singlet−triplet gap, each scheme predicts it to be positive. Although it provides a decent singlet−triplet gap value, SF-ADC(2)-x seems to particularly struggle with the singlet excited states (1^1A_{1g} and 1^1B_{2g}), especially for the doubly excited state 1^1A_{1g} where it underestimates the vertical excitation energy by 0.4 eV. Again, averaging the SF-ADC(2)-s and SF-ADC(3) transition energies is beneficial in most cases with the exception of 1^1A_{1g}. Although the basis set effects are larger than at the SF-TD-DFT level, they remain quite moderate at the SF-ADC level, and this holds for wave function methods in general. Concerning the SF-EOM-CCSD excitation energies at the D_{4h} square-planar equilibrium geometry, very similar conclusions to the ones provided in the previous section dealing with the excitation energies at the D_{2h} rectangular equilibrium geometry can be drawn: (i) SF-EOM-CCSD systematically and consistently overestimates the TBEs by approximately 0.2 eV and is less accurate than SF-ADC(2)-s, (ii) the noniterative triples corrections tend to give a better agreement with respect to the TBE (see the Supporting Information), and (iii) the (dT) correction performs better than the (fT) one.

Let us turn to the multireference results (Table 6). For both active spaces, expectedly, CASSCF does not provide a quantitive energetic description, although it is worth mentioning that the right state ordering is preserved. This is, of course, magnified with the (4e,4o) active space for which the second-order perturbative treatment is unable to provide a satisfying description due to the limited active space. In particular, SC-NEVPT2(4,4)/aug-cc-pVTZ and PC-NEVPT2(4,4)/aug-cc-pVTZ underestimate the singlet−triplet gap by 0.072 and 0.097 eV and, more importantly, flip the ordering of 1^1A_{1g} and 1^1B_{2g}. Although 1^1A_{1g} is not badly described, the excitation energy of the ionic state 1^1B_{2g} is off by almost 1 eV. Thanks to the IPEA shift in CASPT2(4,4), the singlet−triplet gap is accurate and the state ordering remains correct, but the ionic state is still far from being well described. The (12e,12o) active space significantly alleviates these effects, and as usual now, the agreement between CASPT2 and NEVPT2 is very much improved for each state, though the accuracy of multireference approaches remains questionable for the ionic state with, e.g., an error up to −0.093 eV at the PC-NEVPT2(12,12)/aug-cc-pVTZ level.

Finally, let us analyze the excitation energies computed with various CC models that are gathered in Table 6. As mentioned in Section 2.B, we remind the reader that these calculations are performed by considering the 1^1A_{1g} state as reference and that, therefore, 1^1B_{1g} and 1^1B_{2g} are obtained as a de-excitation and an excitation, respectively. Consequently, with respect to 1^1A_{1g}, 1^1B_{1g} has a dominant double excitation character, while 1^1B_{2g} has a dominant single excitation character. This explains why one observes a slower convergence of the transition energies in the case of 1^1B_{1g}, as shown in Figure 4. It is clear from the results of Table 6 that, if one wants to reach high accuracy with such a computational strategy, it is mandatory to include quadruple excitations. Indeed, at the CCSDT/aug-cc-pVTZ level, the singlet−triplet gap is already very accurate (off by 0.005 eV only), while the excitation energies of the singlet states are still 0.131 and 0.688 eV away from their respective TBE. These deviations drop to 0.011 and −0.013 eV at the CC4/aug-cc-pVTZ level. As a final comment, we can note that the CCSDTQ-based TBEs and the CIPSI results are consistent if one takes into account the extrapolation error (see Section 2.A).

4. CONCLUSIONS

In the present study, we have benchmarked a larger number of computational methods on the automerization barrier and the vertical excitation energies of cyclobutadiene in its square (D_{4h}) and rectangular (D_{2h}) geometries, for which we have defined theoretical best estimates based on extrapolated CCSDTQ/aug-cc-pVTZ data.

https://doi.org/10.1021/acs.jpca.2c02480
J. Phys. Chem. A 2022, 126, 4664−4679

Table 6. Vertical Excitation Energies (with Respect to the 1^1B_{1g} Ground State) of the 1^3A_{2g}, 1^1A_{1g}, and 1^1B_{2g} States of CBD at the D_{4h} Square-Planar Equilibrium Geometry of the 1^3A_{2g} State[g]

		excitation energies (eV)		
method	basis	1^3A_{2g}	1^1A_{1g}	1^1B_{2g}
CASSCF(4,4)	6-31+G(d)	0.447	2.257	3.549
	aug-cc-pVDZ	0.438	2.240	3.443
	aug-cc-pVTZ	0.434	2.234	3.424
	aug-cc-pVQZ	0.435	2.235	3.427
CASPT2(4,4)	6-31+G(d)	0.176	1.588	1.899
	aug-cc-pVDZ	0.137	1.540	1.708
	aug-cc-pVTZ	0.128	1.506	1.635
	aug-cc-pVQZ	0.128	1.498	1.612
SC-NEVPT2(4,4)	6-31+G(d)	0.083	1.520	1.380
	aug-cc-pVDZ	0.037	1.465	1.140
	aug-cc-pVTZ	0.024	1.428	1.055
	aug-cc-pVQZ	0.024	1.420	1.030
PC-NEVPT2(4,4)	6-31+G(d)	0.085	1.496	1.329
	aug-cc-pVDZ	0.039	1.440	1.088
	aug-cc-pVTZ	0.026	1.403	1.003
	aug-cc-pVQZ	0.026	1.395	0.977
CASSCF(12,12)	6-31+G(d)	0.386	1.974	2.736
	aug-cc-pVDZ	0.374	1.947	2.649
	aug-cc-pVTZ	0.370	1.943	2.634
	aug-cc-pVQZ	0.371	1.945	2.637
CASPT2(12,12)	6-31+G(d)	0.235	1.635	2.170
	aug-cc-pVDZ	0.203	1.588	2.015
	aug-cc-pVTZ	0.183	1.538	1.926
	aug-cc-pVQZ	0.179	1.522	1.898
SC-NEVPT2(12,12)	6-31+G(d)	0.218	1.644	2.143
	aug-cc-pVDZ	0.189	1.600	1.991
	aug-cc-pVTZ	0.165	1.546	1.892
	aug-cc-pVQZ	0.160	1.529	1.862
PC-NEVPT2(12,12)	6-31+G(d)	0.189	1.579	2.020
	aug-cc-pVDZ	0.156	1.530	1.854
	aug-cc-pVTZ	0.131	1.476	1.756
	aug-cc-pVQZ	0.126	1.460	1.727
CCSD	6-31+G(d)	0.148	1.788	
	aug-cc-pVDZ	0.100	1.650	
	aug-cc-pVTZ	0.085	1.600	
	aug-cc-pVQZ	0.084	1.588	
CC3	6-31+G(d)		1.809	2.836
	aug-cc-pVDZ		1.695	2.646
	aug-cc-pVTZ		1.662	2.720
CCSDT	6-31+G(d)	0.210	1.751	2.565
	aug-cc-pVDZ	0.165	1.659	2.450
	aug-cc-pVTZ	0.149	1.631	2.537
CC4	6-31+G(d)		1.604	2.121
	aug-cc-pVDZ		1.539	1.934
	aug-cc-pVTZ		[1.511][a]	[1.836][b]
CCSDTQ	6-31+G(d)	0.205	1.593	2.134
	aug-cc-pVDZ	[0.160][c]	[1.528][d]	[1.947][d]
	aug-cc-pVTZ	[**0.144**][e]	[**1.500**][f]	[**1.849**][f]
CIPSI	6-31+G(d)	0.201 ± 0.003	1.602 ± 0.007	2.13 ± 0.04
	aug-cc-pVDZ	0.157 ± 0.003	1.587 ± 0.005	2.102 ± 0.027
	aug-cc-pVTZ	0.17 ± 0.03	1.63 ± 0.05	

[a]Value obtained using CC4/aug-cc-pVDZ corrected by the difference between CCSDT/aug-cc-pVTZ and CCSDT/aug-cc-pVDZ. [b]Value obtained using CC4/aug-cc-pVDZ corrected by the difference between PC-NEVPT2(12,12)/aug-cc-pVTZ and PC-NEVPT2(12,12)/aug-cc-pVDZ. [c]Value obtained using CCSDTQ/6-31+G(d) corrected by the difference between CCSDT/aug-cc-pVDZ and CCSDT/6-31+G(d). [d]Value obtained using CCSDTQ/6-31+G(d) corrected by the difference between CC4/aug-cc-pVDZ and CC4/6-31+G(d). [e]TBE value obtained using CCSDTQ/aug-cc-pVDZ corrected by the difference between CCSDT/aug-cc-pVTZ and CCSDT/aug-cc-pVDZ. [f]TBE value obtained using CCSDTQ/aug-cc-pVDZ corrected by the difference between CC4/aug-cc-pVTZ and CC4/aug-cc-pVDZ. [g]The values in square brackets have been obtained by extrapolation via the procedure described in the corresponding footnote. The TBE/aug-cc-pVTZ values are highlighted in bold.

https://doi.org/10.1021/acs.jpca.2c02480
J. Phys. Chem. A 2022, 126, 4664−4679

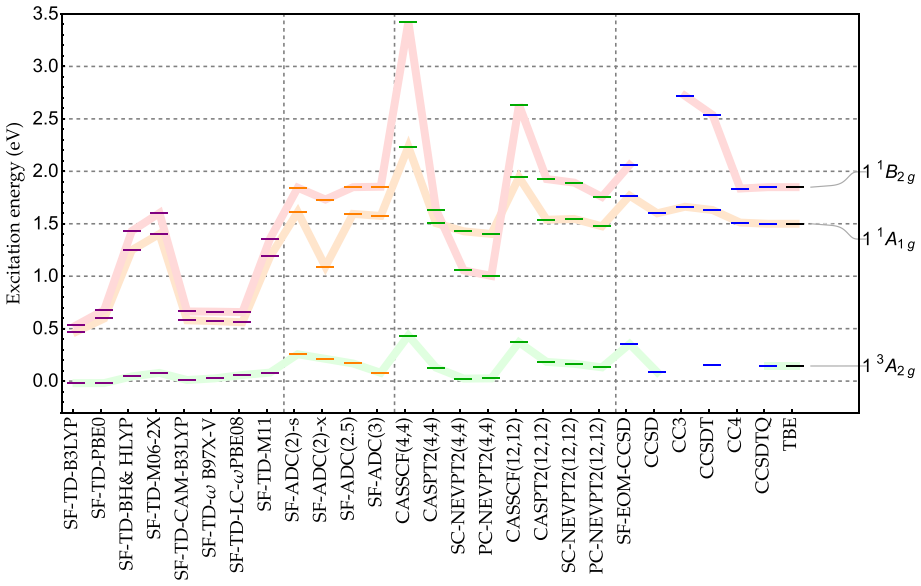

Figure 4. Vertical excitation energies (in eV) of the 1^3A_{2g}, 1^1A_{1g}, and 1^1B_{2g} states at the D_{4h} square-planar equilibrium geometry of the 1^3A_{2g} state using the aug-cc-pVTZ basis. See the Supporting Information for the raw data.

The main take-home messages of the present work can be summarized as follows:

- Within the SF-TD-DFT framework, we advise to use exchange-correlation (hybrids or range-separated hybrids) with a large fraction of short-range exact exchange. This has been shown to be clearly beneficial for the automerization barrier and the vertical excitation energies computed on both the D_{2h} and D_{4h} equilibrium geometries.
- At the SF-ADC level, we have found that, as expected, the extended scheme, SF-ADC(2)-x, systematically worsens the results compared to the cheaper standard version, SF-ADC(2)-s. Moreover, as previously reported, SF-ADC(2)-s and SF-ADC(3) have opposite error patterns which means that SF-ADC(2.5) emerges as an excellent compromise.
- SF-EOM-CCSD shows a similar performance as the cheaper SF-ADC(2)-s formalism, especially for the excitation energies. As previously reported, the two variants including noniterative triples corrections, SF-EOM-CCSD(dT) and SF-EOM-CCSD(fT), improve the results, with the (dT) correction performing slightly better for the vertical excitation energies computed at the D_{2h} and D_{4h} equilibrium geometries.
- For the D_{4h} square-planar structure, a faithful energetic description of the excited states is harder to reach at the SF-TD-DFT level because of the strong multiconfigurational character. In such a scenario, the SF-TD-DFT excitation energies can exhibit errors of the order of 1 eV compared to the TBEs. However, it was satisfying to see that the spin-flip version of ADC can lower these errors to 0.1−0.2 eV.
- Concerning the multireference methods, we have found that while NEVPT2 and CASPT2 can provide different excitation energies for the small (4e,4o) active space, the results become highly similar when the larger (12e,12o) active space is considered. From a more general perspective, a significant difference between NEVPT2 and CASPT2 is usually not a good omen and can be seen as a clear warning sign that the active space is too small or poorly chosen. The ionic states remain a struggle for both CASPT2 and NEVPT2, even with the (12e,12o) active space.
- In the context of CC methods, although the inclusion of triple excitations (via CC3 or CCSDT) yields very satisfactory results in most cases, the inclusion of quadruples excitation (via CC4 or CCSDTQ) is mandatory to reach high accuracy (especially in the case of doubly excited states). Finally, we point out that, considering the error bar related to the CIPSI extrapolation procedure, CCSDTQ and CIPSI yield equivalent excitation energies, hence confirming the outstanding accuracy of CCSDTQ in the context of molecular excited states.

■ ASSOCIATED CONTENT

Supporting Information

The Supporting Information is available free of charge at https://pubs.acs.org/doi/10.1021/acs.jpca.2c02480.

Raw data, additional calculations and geometries, and Cartesian coordinates of various optimized geometries (PDF)

■ AUTHOR INFORMATION

Corresponding Authors

Enzo Monino − *Laboratoire de Chimie et Physique Quantiques (UMR 5626), Université de Toulouse, CNRS, UPS, 31062 Toulouse, France*; Email: emonino@irsamc.ups-tlse.fr

Pierre-François Loos − *Laboratoire de Chimie et Physique Quantiques (UMR 5626), Université de Toulouse, CNRS, UPS, 31062 Toulouse, France*; orcid.org/0000-0003-0598-7425; Email: loos@irsamc.ups-tlse.fr

Authors

Martial Boggio-Pasqua − *Laboratoire de Chimie et Physique Quantiques (UMR 5626), Université de Toulouse, CNRS, UPS, 31062 Toulouse, France*; orcid.org/0000-0001-6684-5223

https://doi.org/10.1021/acs.jpca.2c02480
J. Phys. Chem. A 2022, 126, 4664−4679

Anthony Scemama − *Laboratoire de Chimie et Physique Quantiques (UMR 5626), Université de Toulouse, CNRS, UPS, 31062 Toulouse, France;* orcid.org/0000-0003-4955-7136

Denis Jacquemin − *Nantes Université, CNRS, CEISAM UMR 6230, F-44000 Nantes, France;* orcid.org/0000-0002-4217-0708

Complete contact information is available at: https://pubs.acs.org/10.1021/acs.jpca.2c02480

Notes

The authors declare no competing financial interest.

■ ACKNOWLEDGMENTS

E.M., A.S., and P.F.L. acknowledge funding from the European Research Council (ERC) under the European Union's Horizon 2020 research and innovation programme (Grant agreement No. 863481). This work used the HPC ressources from CALMIP (Toulouse) under allocation 2022-18005 and from the CCIPL center (Nantes).

■ REFERENCES

(1) Bernardi, F.; De, S.; Olivucci, M.; Robb, M. A. The Mechanism of Ground-State-Forbidden Photochemical Pericyclic Reactions: Evidence for Real Conical Intersections. *J. Am. Chem. Soc.* **1990**, *112*, 1737−1744.

(2) Bernardi, F.; Olivucci, M.; Robb, M. A. Potential Energy Surface Crossings in Organic Photochemistry. *Chem. Soc. Rev.* **1996**, *25*, 321−328.

(3) Boggio-Pasqua, M.; Bearpark, M. J.; Robb, M. A. Toward a Mechanistic Understanding of the Photochromism of Dimethyldihydropyrenes. *J. Org. Chem.* **2007**, *72*, 4497−4503.

(4) Klessinger, M.; Michl, J. *Excited States and Photochemistry of Organic Molecules*; VCH: New York, 1995.

(5) Olivucci, M. *Computational Photochemistry*; Elsevier Science: Amsterdam; Boston (Mass.); Paris, 2010.

(6) Robb, M. A.; Garavelli, M.; Olivucci, M.; Bernardi, F. In *Reviews in Computational Chemistry*; Lipkowitz, K. B., Boyd, D. B., Eds.; John Wiley & Sons, Inc.: Hoboken, NJ, USA, 2007; pp 87−146, DOI: 10.1002/9780470125922.ch2.

(7) Van der Lugt, W. T. A. M.; Oosterhoff, L. J. Symmetry Control and Photoinduced Reactions. *J. Am. Chem. Soc.* **1969**, *91*, 6042−6049.

(8) Kancherla, R.; Muralirajan, K.; Sagadevan, A.; Rueping, M. Visible Light-Induced Excited-State Transition-Metal Catalysis. *Trends Chem.* **2019**, *1*, 510−523.

(9) Delgado, J. L.; Bouit, P.-A.; Filippone, S.; Herranz, M.; Martín, N. Organic Photovoltaics: A Chemical Approach. *Chem. Commun.* **2010**, *46*, 4853−4865.

(10) Roos, B. O.; Andersson, K.; Fulscher, M. P.; Malmqvist, P.-â.; Serrano-Andrés, L.; Pierloot, K.; Merchán, M. *Advances in Chemical Physics*; John Wiley & Sons, Ltd.: 1996; pp 219−331, DOI: 10.1002/9780470141526.ch5.

(11) Piecuch, P.; Kowalski, K.; Pimienta, I. S. O.; Mcguire, M. J. Recent Advances in Electronic Structure Theory: Method of Moments of Coupled-Cluster Equations and Renormalized Coupled-Cluster Approaches. *Int. Rev. Phys. Chem.* **2002**, *21*, 527−655.

(12) Dreuw, A.; Head-Gordon, M. Single-Reference Ab Initio Methods for the Calculation of Excited States of Large Molecules. *Chem. Rev.* **2005**, *105*, 4009−4037.

(13) Krylov, A. I. Spin-Flip Equation-of-Motion Coupled-Cluster Electronic Structure Method for a Description of Excited States, Bond Breaking, Diradicals, and Triradicals. *Acc. Chem. Res.* **2006**, *39*, 83−91.

(14) Sneskov, K.; Christiansen, O. Excited State Coupled Cluster Methods. *WIREs Comput. Mol. Sci.* **2012**, *2*, 566−584.

(15) González, L.; Escudero, D.; Serrano-Andrès, L. Progress and Challenges in the Calculation of Electronic Excited States. *ChemPhysChem* **2012**, *13*, 28−51.

(16) Laurent, A. D.; Jacquemin, D. TD-DFT Benchmarks: A Review. *Int. J. Quantum Chem.* **2013**, *113*, 2019−2039.

(17) Adamo, C.; Jacquemin, D. The Calculations of Excited-State Properties with Time-Dependent Density Functional Theory. *Chem. Soc. Rev.* **2013**, *42*, 845−856.

(18) Dreuw, A.; Wormit, M. The Algebraic Diagrammatic Construction Scheme for the Polarization Propagator for the Calculation of Excited States. *WIREs Comput. Mol. Sci.* **2015**, *5*, 82−95.

(19) Ghosh, S.; Verma, P.; Cramer, C. J.; Gagliardi, L.; Truhlar, D. G. Combining Wave Function Methods with Density Functional Theory for Excited States. *Chem. Rev.* **2018**, *118*, 7249−7292.

(20) Blase, X.; Duchemin, I.; Jacquemin, D.; Loos, P. F. The Bethe-Salpeter Formalism: From Physics to Chemistry. *J. Phys. Chem. Lett.* **2020**, *11*, 7371−7382.

(21) Loos, P. F.; Scemama, A.; Jacquemin, D. The Quest for Highly-Accurate Excitation Energies: A Computational Perspective. *J. Phys. Chem. Lett.* **2020**, *11*, 2374−2383.

(22) Hait, D.; Head-Gordon, M. Orbital Optimized Density Functional Theory for Electronic Excited States. *J. Phys. Chem. Lett.* **2021**, *12*, 4517−4529.

(23) Zobel, J. P.; González, L. The Quest to Simulate Excited-State Dynamics of Transition Metal Complexes. *JACS Au* **2021**, *1*, 1116−1140.

(24) Bally, T.; Masamune, S. Cyclobutadiene. *Tetrahedron* **1980**, *36*, 343−370.

(25) Minkin, V. I.; Glukhovtsev, M. N.; Simkin, B. Y. *Aromaticity and Antiaromaticity: Electronic and Structural Aspects*; Wiley; 1994.

(26) Baeyer, A. Ueber Polyacetylenverbindungen. *Berichte Dtsch. Chem. Ges.* **1885**, *18*, 2269−2281.

(27) Reeves, P. C.; Henery, J.; Pettit, R. Further Experiments Pertaining to the Ground State of Cyclobutadiene. *J. Am. Chem. Soc.* **1969**, *91*, 5888−5890.

(28) Irngartinger, H.; Nixdorf, M. Bonding Electron Density Distribution in Tetra-tert-butylcyclobutadiene— A Molecule with an Obviously Non-Square Four-Membered Ring. *Angew. Chem., Int. Ed. Engl.* **1983**, *22*, 403−404.

(29) Ermer, O.; Heilbronner, E. Three Arguments Supporting a Rectangular Structure for Tetra-tert-butylcyclobutadiene. *Angew. Chem., Int. Ed. Engl.* **1983**, *22*, 402−403.

(30) Kreile, J.; Münzel, N.; Schweig, A.; Specht, H. Uv Photoelectron Spectrum of Cyclobutadiene. Free Cyclobutadiene Stable up to High Temperatures. *Chem. Phys. Lett.* **1986**, *124*, 140−146.

(31) Whitman, D. W.; Carpenter, B. K. Limits on the Activation Parameters for Automerization of Cyclobutadiene-1,2-D2. *J. Am. Chem. Soc.* **1982**, *104*, 6473−6474.

(32) Eckert-Maksić, M.; Vazdar, M.; Barbatti, M.; Lischka, H.; Maksić, Z. B. Automerization Reaction of Cyclobutadiene and Its Barrier Height: An Ab Initio Benchmark Multireference Average-Quadratic Coupled Cluster Study. *J. Chem. Phys.* **2006**, *125*, 064310.

(33) Li, X.; Paldus, J. Accounting for the Exact Degeneracy and Quasidegeneracy in the Automerization of Cyclobutadiene via Multireference Coupled-Cluster Methods. *J. Chem. Phys.* **2009**, *131*, 114103.

(34) Shen, J.; Piecuch, P. Combining Active-Space Coupled-Cluster Methods with Moment Energy Corrections via the CC(P;Q) Methodology, with Benchmark Calculations for Biradical Transition States. *J. Chem. Phys.* **2012**, *136*, 144104.

(35) Zhang, T.; Li, C.; Evangelista, F. A. Improving the Efficiency of the Multireference Driven Similarity Renormalization Group via Sequential Transformation, Density Fitting, and the Noninteracting Virtual Orbital Approximation. *J. Chem. Theory Comput.* **2019**, *15*, 4399−4414.

(36) Loos, P.-F.; Boggio-Pasqua, M.; Scemama, A.; Caffarel, M.; Jacquemin, D. Reference Energies for Double Excitations. *J. Chem. Theory Comput.* **2019**, *15*, 1939−1956.

(37) Runge, E.; Gross, E. K. U. Density-Functional Theory for Time-Dependent Systems. *Phys. Rev. Lett.* **1984**, *52*, 997−1000.
(38) Casida, M. E. *Recent Advances in Density Functional Methods*; Recent Advances in Computational Chemistry; World Scientific: 1995; Vol. *1*, pp 155−192, DOI: 10.1142/9789812830586_0005.
(39) Tozer, D. J.; Handy, N. C. On the Determination of Excitation Energies Using Density Functional Theory. *Phys. Chem. Chem. Phys.* **2000**, *2*, 2117−2121.
(40) Maitra, N. T.; Cave, R. J.; Burke, K.; Zhang, F. Double Excitations within Time-Dependent Density Functional Theory Linear Response. *J. Chem. Phys.* **2004**, *120*, 5932−5937.
(41) Cave, R. J.; Zhang, F.; Maitra, N. T.; Burke, K. A Dressed TDDFT Treatment of the 21Ag States of Butadiene and Hexatriene. *Chem. Phys. Lett.* **2004**, *389*, 39−42.
(42) Levine, B. G.; Ko, C.; Quenneville, J.; Martínez, T. J. Conical Intersections and Double Excitations in Time-Dependent Density Functional Theory. *Mol. Phys.* **2006**, *104*, 1039−1051.
(43) Elliott, P.; Goldson, S.; Canahui, C.; Maitra, N. T. Perspectives on Double-Excitations in TDDFT. *Chem. Phys.* **2011**, *391*, 110−119.
(44) Maitra, N. T. In *Fundamentals of Time-Dependent Density Functional Theory*; Marques, M. A., Maitra, N. T., Nogueira, F. M., Gross, E., Rubio, A., Eds.; Springer Berlin Heidelberg: Berlin, Heidelberg, 2012; Vol. *837*, pp 167−184, DOI: 10.1007/978-3-642-23518-4_8.
(45) Maitra, N. T. Charge Transfer in Time-Dependent Density Functional Theory. *J. Phys. Cond. Matt.* **2017**, *29*, 423001.
(46) Kucharski, S. A.; Bartlett, R. J. Recursive Intermediate Factorization and Complete Computational Linearization of the Coupled-Cluster Single, Double, Triple, and Quadruple Excitation Equations. *Theoret. Chim. Acta* **1991**, *80*, 387−405.
(47) Kállay, M.; Gauss, J. Calculation of Excited-State Properties Using General Coupled-Cluster and Configuration-Interaction Models. *J. Chem. Phys.* **2004**, *121*, 9257−9269.
(48) Hirata, S.; Bartlett, R. J. High-Order Coupled-Cluster Calculations through Connected Octuple Excitations. *Chem. Phys. Lett.* **2000**, *321*, 216−224.
(49) Hirata, S. Higher-Order Equation-of-Motion Coupled-Cluster Methods. *J. Chem. Phys.* **2004**, *121*, 51−59.
(50) Andersson, K.; Malmqvist, P. A.; Roos, B. O.; Sadlej, A. J.; Wolinski, K. Second-Order Perturbation Theory with a CASSCF Reference Function. *J. Phys. Chem.* **1990**, *94*, 5483−5488.
(51) Andersson, K.; Malmqvist, P.-A.; Roos, B. O. Second-Order Perturbation Theory with a Complete Active Space Self-Consistent Field Reference Function. *J. Chem. Phys.* **1992**, *96*, 1218−1226.
(52) Roos, B. O.; Fülscher, M.; Malmqvist, P.-Å.; Merchán, M.; Serrano-Andrés, L. *Quantum Mechanical Electronic Structure Calculations with Chemical Accuracy*; Springer Netherlands: Dordrecht, 1995; pp 357−438, DOI: 10.1007/978-94-011-0193-6_8.
(53) Angeli, C.; Cimiraglia, R.; Malrieu, J.-P. N-Electron Valence State Perturbation Theory: A Fast Implementation of the Strongly Contracted Variant. *Chem. Phys. Lett.* **2001**, *350*, 297−305.
(54) Angeli, C.; Cimiraglia, R.; Evangelisti, S.; Leininger, T.; Malrieu, J.-P. Introduction of N-Electron Valence States for Multireference Perturbation Theory. *J. Chem. Phys.* **2001**, *114*, 10252−10264.
(55) Angeli, C.; Cimiraglia, R.; Malrieu, J.-P. N-Electron Valence State Perturbation Theory: A Spinless Formulation and an Efficient Implementation of the Strongly Contracted and of the Partially Contracted Variants. *J. Chem. Phys.* **2002**, *117*, 9138−9153.
(56) Rowe, D. J. Equations-of-Motion Method and the Extended Shell Model. *Rev. Mod. Phys.* **1968**, *40*, 153−166.
(57) Stanton, J. F.; Bartlett, R. J. The Equation of Motion Coupled-cluster Method. A Systematic Biorthogonal Approach to Molecular Excitation Energies, Transition Probabilities, and Excited State Properties. *J. Chem. Phys.* **1993**, *98*, 7029−7039.
(58) Kállay, M.; Gauss, J.; Szalay, P. G. Analytic First Derivatives for General Coupled-Cluster and Configuration Interaction Models. *J. Chem. Phys.* **2003**, *119*, 2991−3004.
(59) Watson, M. A.; Chan, G. K.-L. Excited States of Butadiene to Chemical Accuracy: Reconciling Theory and Experiment. *J. Chem. Theory Comput.* **2012**, *8*, 4013−4018.
(60) Loos, P. F.; Scemama, A.; Blondel, A.; Garniron, Y.; Caffarel, M.; Jacquemin, D. A Mountaineering Strategy to Excited States: Highly-accurate Reference Energies and Benchmarks. *J. Chem. Theory Comput.* **2018**, *14*, 4360−4379.
(61) Loos, P. F.; Lipparini, F.; Boggio-Pasqua, M.; Scemama, A.; Jacquemin, D. A Mountaineering Strategy to Excited States: Highly-accurate Energies and Benchmarks for Medium Size Molecules. *J. Chem. Theory Comput.* **2020**, *16*, 1711−1741.
(62) Jeziorski, B.; Monkhorst, H. J. Coupled-Cluster Method for Multideterminantal Reference States. *Phys. Rev. A* **1981**, *24*, 1668−1681.
(63) Mahapatra, U. S.; Datta, B.; Mukherjee, D. A State-Specific Multi-Reference Coupled Cluster Formalism with Molecular Applications. *Mol. Phys.* **1998**, *94*, 157−171.
(64) Mahapatra, U. S.; Datta, B.; Mukherjee, D. A Size-Consistent State-Specific Multireference Coupled Cluster Theory: Formal Developments and Molecular Applications. *J. Chem. Phys.* **1999**, *110*, 6171−6188.
(65) Lyakh, D. I.; Musiał, M.; Lotrich, V. F.; Bartlett, R. J. Multireference Nature of Chemistry: The Coupled-Cluster View. *Chem. Rev.* **2012**, *112*, 182−243.
(66) Köhn, A.; Hanauer, M.; Mück, L. A.; Jagau, T.-C.; Gauss, J. State-Specific Multireference Coupled-Cluster Theory. *WIREs Comput. Mol. Sci.* **2013**, *3*, 176−197.
(67) Bender, C. F.; Davidson, E. R. Studies in Configuration Interaction: The First-Row Diatomic Hydrides. *Phys. Rev.* **1969**, *183*, 23−30.
(68) Whitten, J. L.; Hackmeyer, M. Configuration Interaction Studies of Ground and Excited States of Polyatomic Molecules. I. The CI Formulation and Studies of Formaldehyde. *J. Chem. Phys.* **1969**, *51*, 5584−5596.
(69) Huron, B.; Malrieu, J. P.; Rancurel, P. Iterative Perturbation Calculations of Ground and Excited State Energies from Multi-configurational Zeroth-order Wavefunctions. *J. Chem. Phys.* **1973**, *58*, 5745−5759.
(70) Giner, E.; Scemama, A.; Caffarel, M. Using Perturbatively Selected Configuration Interaction in Quantum Monte Carlo Calculations. *Can. J. Chem.* **2013**, *91*, 879−885.
(71) Evangelista, F. A. Adaptive Multiconfigurational Wave Functions. *J. Chem. Phys.* **2014**, *140*, 124114.
(72) Giner, E.; Scemama, A.; Caffarel, M. Fixed-Node Diffusion Monte Carlo Potential Energy Curve of the Fluorine Molecule F2 Using Selected Configuration Interaction Trial Wavefunctions. *J. Chem. Phys.* **2015**, *142*, 044115.
(73) Caffarel, M.; Applencourt, T.; Giner, E.; Scemama, A. *Recent Progress in Quantum Monte Carlo*; Chapter 2, pp 15−46, DOI: 10.1021/bk-2016-1234.ch002.
(74) Holmes, A. A.; Changlani, H. J.; Umrigar, C. J. Efficient Heat-Bath Sampling in Fock Space. *J. Chem. Theory Comput.* **2016**, *12*, 1561−1571.
(75) Tubman, N. M.; Lee, J.; Takeshita, T. Y.; Head-Gordon, M.; Whaley, K. B. A Deterministic Alternative to the Full Configuration Interaction Quantum Monte Carlo Method. *J. Chem. Phys.* **2016**, *145*, 044112.
(76) Liu, W.; Hoffmann, M. R. iCI: Iterative CI toward Full CI. *J. Chem. Theory Comput* **2016**, *12*, 1169−1178.
(77) Ohtsuka, Y.; Hasegawa, J.-y. Selected Configuration Interaction Method Using Sampled First-Order Corrections to Wave Functions. *J. Chem. Phys.* **2017**, *147*, 034102.
(78) Zimmerman, P. M. Incremental Full Configuration Interaction. *J. Chem. Phys.* **2017**, *146*, 104102.
(79) Coe, J. P. Machine Learning Configuration Interaction. *J. Chem. Theory Comput.* **2018**, *14*, 5739−5749.
(80) Garniron, Y.; Scemama, A.; Giner, E.; Caffarel, M.; Loos, P. F. Selected Configuration Interaction Dressed by Perturbation. *J. Chem. Phys.* **2018**, *149*, 064103.

(81) Caffarel, M.; Giner, E.; Scemama, A.; Ramírez-Solís, A. Spin Density Distribution in Open-Shell Transition Metal Systems: A Comparative Post-Hartree−Fock, Density Functional Theory, and Quantum Monte Carlo Study of the $CuCl_2$ Molecule. *J. Chem. Theory Comput.* **2014**, *10*, 5286−5296.
(82) Caffarel, M.; Applencourt, T.; Giner, E.; Scemama, A. Communication: Toward an Improved Control of the Fixed-Node Error in Quantum Monte Carlo: The Case of the Water Molecule. *J. Chem. Phys.* **2016**, *144*, 151103.
(83) Scemama, A.; Applencourt, T.; Giner, E.; Caffarel, M. Quantum Monte Carlo with Very Large Multideterminant Wavefunctions. *J. Comput. Chem.* **2016**, *37*, 1866−1875.
(84) Holmes, A. A.; Umrigar, C. J.; Sharma, S. Excited States Using Semistochastic Heat-Bath Configuration Interaction. *J. Chem. Phys.* **2017**, *147*, 164111.
(85) Li, J.; Otten, M.; Holmes, A. A.; Sharma, S.; Umrigar, C. J. Fast Semistochastic Heat-Bath Configuration Interaction. *J. Chem. Phys.* **2018**, *149*, 214110.
(86) Scemama, A.; Garniron, Y.; Caffarel, M.; Loos, P.-F. Deterministic Construction of Nodal Surfaces within Quantum Monte Carlo: The Case of FeS. *J. Chem. Theory Comput.* **2018**, *14*, 1395−1402.
(87) Scemama, A.; Benali, A.; Jacquemin, D.; Caffarel, M.; Loos, P.-F. Excitation Energies from Diffusion Monte Carlo Using Selected Configuration Interaction Nodes. *J. Chem. Phys.* **2018**, *149*, 034108.
(88) Li, J.; Yao, Y.; Holmes, A. A.; Otten, M.; Sun, Q.; Sharma, S.; Umrigar, C. J. Accurate Many-Body Electronic Structure near the Basis Set Limit: Application to the Chromium Dimer. *Phys. Rev. Research* **2020**, *2*, 012015.
(89) Chien, A. D.; Holmes, A. A.; Otten, M.; Umrigar, C. J.; Sharma, S.; Zimmerman, P. M. Excited States of Methylene, Polyenes, and Ozone from Heat-Bath Configuration Interaction. *J. Phys. Chem. A* **2018**, *122*, 2714−2722.
(90) Loos, P. F.; Scemama, A.; Boggio-Pasqua, M.; Jacquemin, D. A Mountaineering Strategy to Excited States: Highly-accurate Energies and Benchmarks for Exotic Molecules and Radicals. *J. Chem. Theory Comput.* **2020**, *16*, 3720−3736.
(91) Loos, P.-F.; Damour, Y.; Scemama, A. The Performance of CIPSI on the Ground State Electronic Energy of Benzene. *J. Chem. Phys.* **2020**, *153*, 176101.
(92) Garniron, Y.; et al. Quantum Package 2.0: An Open-Source Determinant-Driven Suite of Programs. *J. Chem. Theory Comput.* **2019**, *15*, 3591−3609.
(93) Eriksen, J. J.; et al. The Ground State Electronic Energy of Benzene. *J. Phys. Chem. Lett.* **2020**, *11*, 8922−8929.
(94) Yao, Y.; Giner, E.; Li, J.; Toulouse, J.; Umrigar, C. J. Almost Exact Energies for the Gaussian-2 Set with the Semistochastic Heat-Bath Configuration Interaction Method. *J. Chem. Phys.* **2020**, *153*, 124117.
(95) Williams, K. T.; Yao, Y.; Li, J.; Chen, L.; Shi, H.; Motta, M.; Niu, C.; Ray, U.; Guo, S.; Anderson, R. J.; et al. Direct Comparison of Many-Body Methods for Realistic Electronic Hamiltonians. *Phys. Rev. X* **2020**, *10*, 011041.
(96) Véril, M.; Scemama, A.; Caffarel, M.; Lipparini, F.; Boggio-Pasqua, M.; Jacquemin, D.; Loos, P.-F. QUESTDB: A Database of Highly Accurate Excitation Energies for the Electronic Structure Community. *WIREs Comput. Mol. Sci.* **2021**, *11*, e1517.
(97) Loos, P.-F.; Matthews, D. A.; Lipparini, F.; Jacquemin, D. How Accurate Are EOM-CC4 Vertical Excitation Energies? *J. Chem. Phys.* **2021**, *154*, 221103.
(98) Damour, Y.; Véril, M.; Kossoski, F.; Caffarel, M.; Jacquemin, D.; Scemama, A.; Loos, P.-F. Accurate Full Configuration Interaction Correlation Energy Estimates for Five- and Six-Membered Rings. *J. Chem. Phys.* **2021**, *155*, 134104.
(99) Garniron, Y.; Scemama, A.; Loos, P.-F.; Caffarel, M. Hybrid Stochastic-Deterministic Calculation of the Second-Order Perturbative Contribution of Multireference Perturbation Theory. *J. Chem. Phys.* **2017**, *147*, 034101.
(100) Krylov, A. I. Size-Consistent Wave Functions for Bond-Breaking: The Equation-of-Motion Spin-Flip Model. *Chem. Phys. Lett.* **2001**, *338*, 375−384.
(101) Krylov, A. I. Spin-Flip Configuration Interaction: An Electronic Structure Model That Is Both Variational and Size-Consistent. *Chem. Phys. Lett.* **2001**, *350*, 522−530.
(102) Krylov, A. I.; Sherrill, C. D. Perturbative Corrections to the Equation-of-Motion Spin−Flip Self-Consistent Field Model: Application to Bond-Breaking and Equilibrium Properties of Diradicals. *J. Chem. Phys.* **2002**, *116*, 3194−3203.
(103) Casanova, D.; Krylov, A. I. Spin-Flip Methods in Quantum Chemistry. *Phys. Chem. Chem. Phys.* **2020**, *22*, 4326−4342.
(104) Sears, J. S.; Sherrill, C. D.; Krylov, A. I. A Spin-Complete Version of the Spin-Flip Approach to Bond Breaking: What Is the Impact of Obtaining Spin Eigenfunctions? *J. Chem. Phys.* **2003**, *118*, 9084−9094.
(105) Casanova, D.; Head-Gordon, M. The Spin-Flip Extended Single Excitation Configuration Interaction Method. *J. Chem. Phys.* **2008**, *129*, 064104.
(106) Huix-Rotllant, M.; Natarajan, B.; Ipatov, A.; Muhavini Wawire, C.; Deutsch, T.; Casida, M. E. Assessment of Noncollinear Spin-Flip Tamm−Dancoff Approximation Time-Dependent Density-Functional Theory for the Photochemical Ring-Opening of Oxirane. *Phys. Chem. Chem. Phys.* **2010**, *12*, 12811.
(107) Li, Z.; Liu, W. Spin-Adapted Open-Shell Random Phase Approximation and Time-Dependent Density Functional Theory. I. Theory. *J. Chem. Phys.* **2010**, *133*, 064106.
(108) Li, Z.; Liu, W.; Zhang, Y.; Suo, B. Spin-Adapted Open-Shell Time-Dependent Density Functional Theory. II. Theory and Pilot Application. *J. Chem. Phys.* **2011**, *134*, 134101.
(109) Li, Z.; Liu, W. Spin-Adapted Open-Shell Time-Dependent Density Functional Theory. III. An Even Better and Simpler Formulation. *J. Chem. Phys.* **2011**, *135*, 194106.
(110) Zhang, X.; Herbert, J. M. Analytic Derivative Couplings in Time-Dependent Density Functional Theory: Quadratic Response Theory versus Pseudo-Wavefunction Approach. *J. Chem. Phys.* **2015**, *142*, 064109.
(111) Lee, S.; Filatov, M.; Lee, S.; Choi, C. H. Eliminating Spin-Contamination of Spin-Flip Time Dependent Density Functional Theory within Linear Response Formalism by the Use of Zeroth-Order Mixed-Reference (MR) Reduced Density Matrix. *J. Chem. Phys.* **2018**, *149*, 104101.
(112) Head-Gordon, M. Characterizing unpaired electrons from the one-particle density matrix. *Chem. Phys. Lett.* **2003**, *372*, 508−511.
(113) Orms, N.; Dirk, R. R.; Andreas, D.; Krylov, A. I. Characterizing Bonding Patterns in Diradicals and Triradicals by Density-Based Wave Function Analysis: A Uniform Approach. *J. Chem. Theory Comput.* **2018**, *14*, 638−648.
(114) Scemama, A.; Caffarel, M.; Benali, A.; Jacquemin, D.; Loos, P. F. Influence of Pseudopotentials on Excitation Energies from Selected Configuration Interaction and Diffusion Monte Carlo. *Res. Chem.* **2019**, *1*, 100002.
(115) Eriksen, J. J. The Shape of Full Configuration Interaction to Come. *J. Phys. Chem. Lett.* **2021**, *12*, 418−432.
(116) Čížek, J. On the Correlation Problem in Atomic and Molecular Systems. Calculation of Wavefunction Components in Ursell-Type Expansion Using Quantum-Field Theoretical Methods. *J. Chem. Phys.* **1966**, *45*, 4256−4266.
(117) Paldus, J.; Cizek, J.; Shavitt, I. Correlation Problems in Atomic and Molecular Systems. IV. Extended Coupled-Pair Many-Electron Theory and Its Application to the bH_3 Molecule. *Phys. Rev. A* **1972**, *5*, 50−67.
(118) Crawford, T. D.; Schaefer, H. F. *Reviews in Computational Chemistry*; John Wiley & Sons, Ltd.: 2000; pp 33−136, DOI: 10.1002/9780470125915.ch2.
(119) Bartlett, R. J.; Musiał, M. Coupled-Cluster Theory in Quantum Chemistry. *Rev. Mod. Phys.* **2007**, *79*, 291−352.
(120) Shavitt, I.; Bartlett, R. J. *Many-Body Methods in Chemistry and Physics: MBPT and Coupled-Cluster Theory*; Cambridge Molecular

Science; Cambridge University Press: Cambridge, 2009; DOI: 10.1017/CBO9780511596834.
(121) Purvis, G. D.; Bartlett, R. J. A Full Coupled-Cluster Singles and Doubles Model: The Inclusion of Disconnected Triples. *J. Chem. Phys.* **1982**, *76*, 1910−1918.
(122) Noga, J.; Bartlett, R. J. The Full CCSDT Model for Molecular Electronic Structure. *J. Chem. Phys.* **1987**, *86*, 7041−7050.
(123) Scuseria, G. E.; Schaefer, H. F. A New Implementation of the Full CCSDT Model for Molecular Electronic Structure. *Chem. Phys. Lett.* **1988**, *152*, 382−386.
(124) Oliphant, N.; Adamowicz, L. Coupled-Cluster Method Truncated at Quadruples. *J. Chem. Phys.* **1991**, *95*, 6645−6651.
(125) Kucharski, S. A.; Bartlett, R. J. Recursive Intermediate Factorization and Complete Computational Linearization of the Coupled-Cluster Single, Double, Triple, and Quadruple Excitation Equations. *Theoret. Chim. Acta* **1991**, *80*, 387−405.
(126) Kucharski, S. A.; Bartlett, R. J. The Coupled-Cluster Single, Double, Triple, and Quadruple Excitation Method. *J. Chem. Phys.* **1992**, *97*, 4282−4288.
(127) Koch, H.; Jensen, H. J. A.; Jorgensen, P.; Helgaker, T. Excitation Energies from the Coupled Cluster Singles and Doubles Linear Response Function (CCSDLR). Applications to Be, CH^+, CO, and H_2O. *J. Chem. Phys.* **1990**, *93*, 3345−3350.
(128) Christiansen, O.; Jørgensen, P.; Hättig, C. Response Functions from Fourier Component Variational Perturbation Theory Applied to a Time-Averaged Quasienergy. *Int. J. Quantum Chem.* **1998**, *68*, 1−52.
(129) Kucharski, S. A.; Włoch, M.; Musiał, M.; Bartlett, R. J. Coupled-Cluster Theory for Excited Electronic States: The Full Equation-of-Motion Coupled-Cluster Single, Double, and Triple Excitation Method. *J. Chem. Phys.* **2001**, *115*, 8263−8266.
(130) Kowalski, K.; Piecuch, P. The Active-Space Equation-of-Motion Coupled-Cluster Methods for Excited Electronic States: Full EOMCCSDt. *J. Chem. Phys.* **2001**, *115*, 643−651.
(131) Christiansen, O.; Koch, H.; Jorgensen, P. Response Functions in the CC3 Iterative Triple Excitation Model. *J. Chem. Phys.* **1995**, *103*, 7429−7441.
(132) Hättig, C.; Weigend, F. CC2 Excitation Energy Calculations on Large Molecules Using the Resolution of the Identity Approximation. *J. Chem. Phys.* **2000**, *113*, 5154−5161.
(133) Koch, H.; Christiansen, O.; Jørgensen, P.; Olsen, J. Excitation Energies of BH, CH2 and Ne in Full Configuration Interaction and the Hierarchy CCS, CC2, CCSD and CC3 of Coupled Cluster Models. *Chem. Phys. Lett.* **1995**, *244*, 75−82.
(134) Kállay, M.; Gauss, J. Approximate Treatment of Higher Excitations in Coupled-Cluster Theory. *J. Chem. Phys.* **2005**, *123*, 214105.
(135) Matthews, D. A.; Cheng, L.; Harding, M. E.; Lipparini, F.; Stopkowicz, S.; Jagau, T.-C.; Szalay, P. G.; Gauss, J.; Stanton, J. F. Coupled-Cluster Techniques for Computational Chemistry: The CFOUR Program Package. *J. Chem. Phys.* **2020**, *152*, 214108.
(136) Aidas, K.; et al. The Dalton Quantum Chemistry Program System. *WIREs Comput. Mol. Sci.* **2014**, *4*, 269−284.
(137) Kállay, M.; et al. The MRCC Program System: Accurate Quantum Chemistry from Water to Proteins. *J. Chem. Phys.* **2020**, *152*, 074107.
(138) Werner, H.-J.; et al. The Molpro Quantum Chemistry Package. *J. Chem. Phys.* **2020**, *152*, 144107.
(139) Davidson, E. R. The Spatial Extent of the v State of Ethylene and Its Relation to Dynamic Correlation in the Cope Rearrangement. *J. Phys. Chem.* **1996**, *100*, 6161−6166.
(140) Angeli, C. On the Nature of the $\pi \rightarrow \pi$ Ionic Excited States: The V State of Ethene as a Prototype. *J. Comput. Chem.* **2009**, *30*, 1319−1333.
(141) Ben Amor, N.; Noûs, C.; Trinquier, G.; Malrieu, J.-P. Spin Polarization as an Electronic Cooperative Effect. *J. Chem. Phys.* **2020**, *153*, 044118.
(142) Roos, B. O.; Andersson, K. Multiconfigurational Perturbation Theory with Level Shift — the Cr_2 Potential Revisited. *Chem. Phys. Lett.* **1995**, *245*, 215−223.
(143) Ghigo, G.; Roos, B. O.; Malmqvist, P.-Å. A Modified Definition of the Zeroth-Order Hamiltonian in Multiconfigurational Perturbation Theory (CASPT2). *Chem. Phys. Lett.* **2004**, *396*, 142−149.
(144) Schapiro, I.; Sivalingam, K.; Neese, F. Assessment of n-Electron Valence State Perturbation Theory for Vertical Excitation Energies. *J. Chem. Theory Comput.* **2013**, *9*, 3567−3580.
(145) Zobel, J. P.; Nogueira, J. J.; Gonzalez, L. The IPEA Dilemma in CASPT2. *Chem. Sci.* **2017**, *8*, 1482−1499.
(146) Sarkar, R.; Loos, P. F.; Boggio-Pasqua, M.; Jacquemin, D. Assessing the Performances of CASPT2 and NEVPT2 for Vertical Excitation Energies. *J. Chem. Theory Comput.* **2022**, *18*, 2418−2436.
(147) Knowles, P. J.; Werner, H.-J. An efficient method for the evaluation of coupling coefficients in configuration interaction calculations. *Chem. Phys. Lett.* **1988**, *145*, 514−522.
(148) Werner, H.; Knowles, P. J. An efficient internally contracted multiconfiguration−reference configuration interaction method. *J. Chem. Phys.* **1988**, *89*, 5803−5814.
(149) Lefrancois, D.; Wormit, M.; Dreuw, A. Adapting Algebraic Diagrammatic Construction Schemes for the Polarization Propagator to Problems with Multi-Reference Electronic Ground States Exploiting the Spin-Flip Ansatz. *J. Chem. Phys.* **2015**, *143*, 124107.
(150) Schirmer, J. Beyond the Random-Phase Approximation: A New Approximation Scheme for the Polarization Propagator. *Phys. Rev. A* **1982**, *26*, 2395−2416.
(151) Trofimov, A. B.; Schirmer, J. Polarization Propagator Study of Electronic Excitation in Key Heterocyclic Molecules I. Pyrrole. *Chem. Phys.* **1997**, *214*, 153−170.
(152) Trofimov, A. B.; Stelter, G.; Schirmer, J. Electron Excitation Energies Using a Consistent Third-Order Propagator Approach: Comparison with Full Configuration Interaction and Coupled Cluster Results. *J. Chem. Phys.* **2002**, *117*, 6402−6410.
(153) Harbach, P. H. P.; Wormit, M.; Dreuw, A. The Third-Order Algebraic Diagrammatic Construction Method (ADC(3)) for the Polarization Propagator for Closed-Shell Molecules: Efficient Implementation and Benchmarking. *J. Chem. Phys.* **2014**, *141*, 064113.
(154) Epifanovsky, E.; et al. Software for the Frontiers of Quantum Chemistry: An Overview of Developments in the Q-Chem 5 Package. *J. Chem. Phys.* **2021**, *155*, 084801.
(155) Loos, P.-F.; Jacquemin, D. Is ADC(3) as Accurate as CC3 for Valence and Rydberg Transition Energies? *J. Phys. Chem. Lett.* **2020**, *11*, 974−980.
(156) Shao, Y.; Head-Gordon, M.; Krylov, A. I. The Spin−Flip Approach within Time-Dependent Density Functional Theory: Theory and Applications to Diradicals. *J. Chem. Phys.* **2003**, *118*, 4807−4818.
(157) Becke, A. D. Density-Functional Exchange-Energy Approximation with Correct Asymptotic Behavior. *Phys. Rev. A* **1988**, *38*, 3098−3100.
(158) Lee, C.; Yang, W.; Parr, R. G. Development of the Colle-Salvetti Correlation-Energy Formula into a Functional of the Electron Density. *Phys. Rev. B* **1988**, *37*, 785−789.
(159) Becke, A. D. Density-Functional Thermochemistry. III. The Role of Exact Exchange. *J. Chem. Phys.* **1993**, *98*, 5648−5652.
(160) Adamo, C.; Barone, V. Toward Reliable Density Functional Methods without Adjustable Parameters: The PBE0Model. *J. Chem. Phys.* **1999**, *110*, 6158−6170.
(161) Ernzerhof, M.; Scuseria, G. E. Assessment of the Perdew−Burke−Ernzerhof Exchange-Correlation Functional. *J. Chem. Phys.* **1999**, *110*, 5029−5036.
(162) Yanai, T.; Tew, D. P.; Handy, N. C. A New Hybrid Exchange−Correlation Functional Using the Coulomb-attenuating Method (CAM-B3LYP). *Chem. Phys. Lett.* **2004**, *393*, 51−57.
(163) Weintraub, E.; Henderson, T. M.; Scuseria, G. E. Long-Range-Corrected Hybrids Based on a New Model Exchange Hole. *J. Chem. Theory Comput.* **2009**, *5*, 754−762.
(164) Mardirossian, N.; Head-Gordon, M. ωB97X-V: A 10-Parameter, Range-Separated Hybrid, Generalized Gradient Approximation Density Functional with Nonlocal Correlation, Designed by a Survival-of-the-Fittest Strategy. *Phys. Chem. Chem. Phys.* **2014**, *16*, 9904−9924.

(165) Zhao, Y.; Truhlar, D. G. The M06 Suite of Density Functionals for Main Group Thermochemistry, Thermochemical Kinetics, Noncovalent Interactions, Excited States, and Transition Elements: Two New Functionals and Systematic Testing of Four M06-class Functionals and 12 Other Functionals. *Theor. Chem. Acc.* **2008**, *120*, 215−241.
(166) Peverati, R.; Truhlar, D. G. Improving the Accuracy of Hybrid Meta-GGA Density Functionals by Range Separation. *J. Phys. Chem. Lett.* **2011**, *2*, 2810−2817.
(167) Hirata, S.; Head-Gordon, M. Time-Dependent Density Functional Theory within the Tamm−Dancoff Approximation. *Chem. Phys. Lett.* **1999**, *314*, 291−299.
(168) Levchenko, S. V.; Krylov, A. I. Equation-of-Motion Spin-Flip Coupled-Cluster Model with Single and Double Substitutions: Theory and Application to Cyclobutadiene. *J. Chem. Phys.* **2004**, *120*, 175−185.
(169) Manohar, P. U.; Krylov, A. I. A Noniterative Perturbative Triples Correction for the Spin-Flipping and Spin-Conserving Equation-of-Motion Coupled-Cluster Methods with Single and Double Substitutions. *J. Chem. Phys.* **2008**, *129*, 194105.
(170) Casanova, D.; Slipchenko, L. V.; Krylov, A. I.; Head-Gordon, M. Double spin-flip approach within equation-of-motion coupled cluster and configuration interaction formalisms: Theory, implementation, and examples. *J. Chem. Phys.* **2009**, *130*, 044103.
(171) Dutta, A. K.; Pal, S.; Ghosh, D. Perturbative approximations to single and double spin flip equation of motion coupled cluster singles doubles methods. *J. Chem. Phys.* **2013**, *139*, 124116.
(172) Mulliken, R. S. Report on Notation for the Spectra of Polyatomic Molecules. *J. Chem. Phys.* **1955**, *23*, 1997−2011.
(173) Dunning, T. H. Gaussian Basis Sets for Use in Correlated Molecular Calculations. I. The Atoms Boron through Neon and Hydrogen. *J. Chem. Phys.* **1989**, *90*, 1007−1023.
(174) Gururangan, K.; Deustua, J. E.; Jun, S.; Piotr, P. High-level coupled-cluster energetics by merging moment expansions with selected configuration interaction. *J. Chem. Phys.* **2021**, *155*, 174114.
(175) Deustua, J. E.; Jun, S.; Piotr, P. High-level coupled-cluster energetics by Monte Carlo sampling and moment expansions: Further details and comparisons. *J. Chem. Phys.* **2021**, *154*, 124103.
(176) Loos, P. F.; Pradines, B.; Scemama, A.; Toulouse, J.; Giner, E. A Density-Based Basis-Set Correction for Wave Function Theory. *J. Phys. Chem. Lett.* **2019**, *10*, 2931−2937.
(177) Wormit, M.; Rehn, D. R.; Harbach, P. H.; Wenzel, J.; Krauter, C. M.; Epifanovsky, E.; Dreuw, A. Investigating excited electronic states using the algebraic diagrammatic construction (ADC) approach of the polarisation propagator. *Mol. Phys.* **2014**, *112*, 774−784.
(178) Giner, E.; Scemama, A.; Toulouse, J.; Loos, P. F. Chemically Accurate Excitation Energies with Small Basis Sets. *J. Chem. Phys.* **2019**, *151*, 144118.

https://doi.org/10.1021/acs.jpca.2c02480
J. Phys. Chem. A 2022, 126, 4664−4679